Budgets of Reactive Nitrogen, Hydrocarbons, and Ozone Over the Amazon Forest during the Wet Season

DANIEL J. JACOB AND STEVEN C. WOFSY

Department of Earth and Planetary Sciences and Division of Applied Sciences,
Harvard University, Cambridge, Massachusetts

The atmospheric composition over the Amazon forest during the wet season is simulated with a one-dimensional photochemical model for the planetary boundary layer (PBL) extending from the ground to 2000-m altitude. The model is constrained and evaluated using observations from the ABLE 2B field expedition. Results indicate that only $\approx 20\%$ of NO_x emitted by soils is exported to the atmosphere above the forest canopy. The balance is deposited to vegetation before leaving the canopy layer. The small NO_x flux that escapes from the canopy is nevertheless sufficient to account for the low NO concentrations observed in the PBL. Decomposition of peroxyacetylnitrate (PAN) supplied from aloft provides only a minor source of NO_x in the PBL, although it could provide the major source of NO_x at higher altitudes. Soil emission can account for only a portion of NO_y observed over the forest. Organic nitrates of nonbiogenic origin likely account for the balance of NO_y. Enhancements of CO observed in the PBL cannot be explained by oxidation of biogenic hydrocarbons, and appear to reflect direct emission of CO by the forest ecosystem. Concentrations of O_3 in the PBL are regulated largely by transport from aloft and deposition to the canopy, with little net influence from photochemistry. Ozone is photochemically produced immediately above the forest where NO concentrations are relatively high, but is photochemically consumed in the upper portion of the PBL.

1. INTRODUCTION

The ABLE 2B field expedition [*Harriss et al.*, this issue (*a*)] has provided a detailed survey of atmospheric composition over the Amazon forest during the wet season. The findings reveal a remarkably pristine atmosphere. Concentrations of NO measured from aircraft were usually less than 10 ppt (A. L. Torres and K. R. Hooks, Nitric oxide measurements over the Amazon Basin: ABLE 2B results, submitted to *Journal of Geophysical Research*, 1989). Concentrations of O_3 at 2000 m altitude averaged 18 ppb [*Browell et al.*, this issue; *Gregory et al.*, this issue; *Kirchhoff et al.*, this issue], and the mean daytime concentration at canopy top was only 6 ppb [*Bakwin et al.*, this issue (*a*)]. The atmospheric composition observed during ABLE 2B reflects influences from photochemical reactions, biosphere-atmosphere exchange, vertical mixing, and long-range transport of pollution. We investigate here these influences, using a one-dimensional (1D) photochemical model for the planetary boundary layer (PBL) extending from the ground to 2000 m. We emphasize factors that regulate the concentrations, transformation rates, and fluxes of hydrocarbons, CO, reactive nitrogen species, and O_3.

Previous model studies of atmospheric chemistry over the Amazon Basin have focused on dry season conditions [*Crutzen et al.*, 1985; *Jacob and Wofsy*, 1988]. A major difference between photochemistry in the wet and dry seasons is that NO concentrations are much lower in the wet season. The background PBL concentrations of NO observed during the ABLE 2A dry season expedition ranged from 10 to 60 ppt [*Torres and Buchan*, 1988], and values up to 250 ppt were observed in fresh biomass burning plumes [*Andreae et al.*, 1988]. The background NO concentrations in the dry season are sufficiently high to allow significant photochemical production of O_3 [*Jacob and Wofsy*, 1988], and this production is enhanced in biomass burning plumes [*Crutzen et al.*, 1985; *Andreae et al.*, 1988; *Kirchhoff et al.*, 1989]. In the wet season, by contrast, we will see that NO concentrations are so low that photochemistry can represent a net sink for O_3.

We have argued previously [*Jacob and Wofsy*, 1988] that the background NO concentrations observed during the dry season could be explained largely by soil emissions of NO. Soil emissions are 5 times lower in the wet season than in the dry season [*Bakwin et al.*, this issue (*b*)], consistent with the observed seasonality of NO concentrations. Our model results, discussed below, indicate that only 20% of NO_x emitted by soil is actually exported to the PBL above the forest; the balance is removed by deposition to vegetation during transport from the ground to the top of the canopy. Nevertheless, we argue that soil emissions can account for most of the NO observed in the PBL during the wet season. We argue further that ventilation of NO_x from the PBL to the free troposphere (above 2000 m) is negligible, implying that soil emissions of NO from the Amazon Basin make little contribution to the global atmospheric budget of reactive nitrogen.

Several authors, including *Crutzen* [1979] and *Singh* [1987], have proposed that thermal decomposition of peroxyacetylnitrate (PAN) could provide an important source of NO_x in low-NO_x atmospheres. In particular, the PAN measurements of *Singh et al.* [this issue] during ABLE 2B suggest that decomposition of PAN could constitute the principal source of NO_x in the free troposphere over the Amazon Basin. The concentrations of PAN were consistently higher in the free troposphere (20-125 ppt) than in the PBL (5-20 ppt), implying a net downward flux of PAN to the PBL. We find however that this flux supplies only a small source of reactive nitrogen to the PBL as compared to soil emissions of NO. Decomposition of PAN to NO_x in the PBL is inhibited by the abundance of peroxyacetyl radicals (CH_3CO_3) produced from atmospheric oxidation of isoprene. Despite the low levels of NO_x, net conversion of NO_x to PAN can take place at midday when CH_3CO_3 levels are maximum.

Photochemical oxidation of NO_x produces HNO_3 and organic nitrates in addition to PAN. The total concentration of reactive oxides of nitrogen (NO_y) measured just above canopy top during ABLE 2B averaged about 450 ppt [*Bakwin et al.*, this issue (*a*)]. Model results indicate that soil emissions of NO cannot account for the observed NO_y concentrations, and we speculate that organic nitrates of nonbiogenic origin make a major contribution to the observed NO_y. Local emissions from Manaus, or long-range tran-

sport of pollution from eastern Brazil and Africa, could be implicated [Andreae et al., this issue (a); Talbot et al., this issue (a)].

Extremely low O_3 concentrations were measured during ABLE 2B [Bakwin et al., this issue (a); Browell et al., this issue; Gregory et al., this issue; Kirchhoff et al., this issue], reflecting the rapid deposition of O_3 to the forest canopy [Fan et al., this issue] and the lack of photochemical production in the PBL. Previous model studies have pointed out the potential for vigorous photochemical loss of O_3 in low-NO_x atmospheres [Fishman et al., 1979; Logan et al., 1981; Liu et al., 1983; Chameides et al., 1987]. These previous studies focused on marine environments, where photochemistry involves principally the oxidation of CO by OH, producing HO_2, and the O_3 yield is largely determined by the relative rates of the HO_2 + NO reaction (producing O_3) and the HO_2 + O_3 reaction (consuming O_3). Different photochemistry is expected over the Amazon forest because of the high concentrations of isoprene. Isoprene provides the principal atmospheric sink for OH in the PBL [Zimmerman et al., 1988; Jacob and Wofsy, 1988], so that rates for O_3 production or loss are determined largely by the fates of the organic peroxy radicals (RO_2) produced from isoprene oxidation. The RO_2 radicals are largely unreactive with O_3 [Atkinson and Lloyd, 1984], in contrast to HO_2. As a result we find that the crossover from net O_3 production to net loss over the Amazon forest takes place at $\approx$ 5 ppt NO, as compared to $\approx$ 10 ppt NO in marine atmospheres [Fishman et al., 1979; Chameides et al., 1987]. The low NO concentration required for O_3 production moderates the potential for photochemical loss of O_3 over the Amazon forest.

The photochemical model developed for the present study includes a detailed mechanism for photochemistry in low-NO_x atmospheres [Lurmann et al., 1986; Jacob and Wofsy, 1988], a 1D simulation of transport within the canopy and in the PBL, and a multilevel resistance-in-series scheme for deposition to vegetation [Shreffler, 1978; Meyers and Baldocchi, 1988]. The model is intended to simulate relatively undisturbed meteorological conditions over the Amazon forest, characterized by a well-defined diurnal cycle of mixed layer growth and decay. Such conditions were observed frequently during ABLE 2B [Browell et al., this issue; Gregory et al., this issue], and were interrupted by occasional very large disturbances [Scala et al., this issue]. The structure of the model is described in section 2. Budgets of O_3 and NO_x within the canopy are examined in section 3. The photochemistry of the PBL is discussed in sections 4-8, with focus on hydrocarbons (section 4), CO (section 5), reactive nitrogen (section 6), odd hydrogen (section 7), and O_3 (section 8). The sensitivity of model results to hydrocarbon levels is investigated in section 9. Concluding remarks are in section 10. Model results for sulfur species and organic acids are presented elsewhere [Andreae et al., this issue (a); Talbot et al., this issue (b)]. Sensitivity model studies focusing on the mechanisms for dry deposition to the Amazon forest, the export of biogenic NO_x out of the forest canopy, and the effects of human colonization are presented in Fan et al. [this issue], Jacob and Bakwin [1990], and Keller et al. [1990], respectively.

2. MODEL DESCRIPTION

2.1. Transport

The model domain is restricted to the vertical, extending from the ground to 2000 m. Some rationale for using a 1D model is provided by the ABLE 2B aircraft observations of O_3 and aerosol distributions over the Amazon Basin, which show relatively little horizontal variation even during cross-Basin flights from Manaus to Belem [Browell et al., this issue; Gregory et al., this issue].

Most of the time, the observed vertical distributions of O_3 and aerosol below 2000 m display a well-defined diurnal pattern of mixed layer growth and decay [Browell et al., this issue; Gregory et al., this issue], which can be reasonably simulated with a 1D model. We focus our attention here on these relatively undisturbed meteorological conditions. The principal drawback of a 1D model is that it cannot simulate the efficient mixing of air to high altitudes that takes place during deep convective events [Chatfield and Delany, 1990]. The rapid redistribution of O_3 observed during such events is examined by Scala et al. [this issue] using a 2D model.

The upper boundary of the model domain at 2000 m is assumed to represent the top of the PBL. The PBL includes an active mixed layer, which grows and decays over the course of the day, and a remnant mixed layer above, which is entrained into the active mixed layer during the morning hours. Observations in the dry season indicate a well-defined PBL, capped at 2500-3000 m by the semi-permanent trade wind inversion [Kousky and Kagano, 1981; Browell et al., 1988; Gregory et al., 1988]. In the wet season the PBL is not as well defined, because the trade wind inversion is absent, however the vertical distributions of various tracers indicate a marked decrease in surface influences above 2000 m. For example, the average O_3 vertical profiles reported by Browell et al. [this issue] show a rapid increase of concentrations with altitude up to 2000 m, reflecting the influence of the surface sink for O_3, but little further increase above. Similarly, the aerosol profiles reported by Gregory et al. [this issue] usually show a rapid decline in concentrations above 2000 m.

The vertical distributions of trace species within the 0-2000 m model domain are resolved with seven grid cells (Figure 1), in-
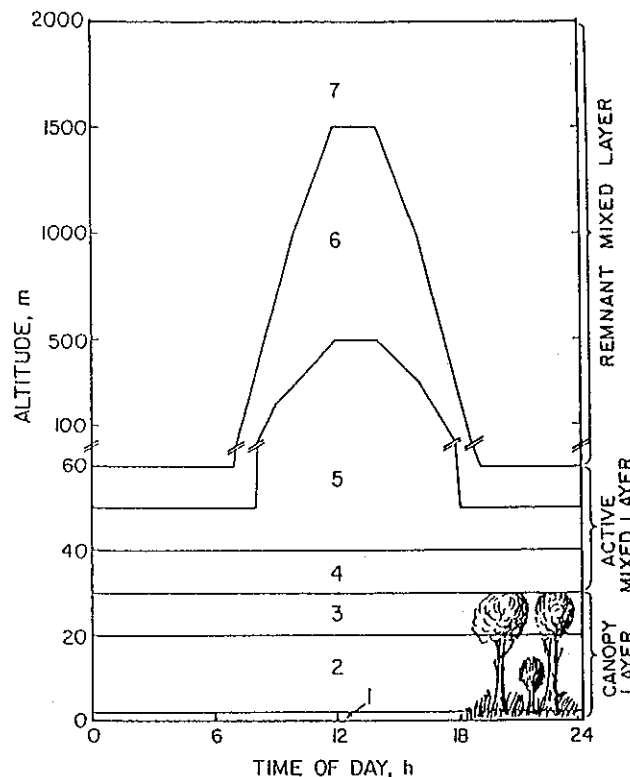

Fig. 1. Vertical structure of the model domain as a function of time of day. The canopy layer (grid cells 1-3) extends from 0 to 30 m, and the PBL (grid cells 4-7) extends from 30 to 2000 m. The tops of grid cells 5 and 6 move with time of day to simulate the growth and decay of the active mixed layer.

'luding three cells in the canopy (0-30 m) and four cells in the BL above the canopy (30-2000 m). The grid cells are assumed to be individually well-mixed. The subdivision of the canopy layer into three grid cells is intended in part to resolve the observed vertical gradients of ^{222}Rn, NO, and O_3 [*Trumbore et al.*, this issue; *Bakwin et al.*, this issue (*a*)], and in part to resolve the vertical distributions of vegetation density and stomatal resistances [*Roberts et al.*, 1990]. The subdivision of the PBL into four grid cells is intended to distinguish the active mixed layer (grid cells 4-6) from the remnant mixed layer (grid cell 7), and to provide some resolution of vertical transport within the active mixed layer.

Grid cells 4-6 in the model simulate the active mixed layer, which is subject to strong turbulence in the daytime due to solar heating of the canopy. The depth of the active mixed layer (top of grid cell 6) is specified on the basis of observed vertical distributions of O_3 and aerosol [*Browell et al.*, this issue; *Gregory et al.*, this issue]. It varies with time of day as a function of the energy balance at canopy top, peaking at about 1500 m at midday. As the active mixed layer grows during the morning hours it entrains air from the remnant mixed layer, and the reverse process (stratification) takes place in the late afternoon as the active mixed layer decays [*Jacob and Wofsy*, 1988]. Entrainment and stratification are simulated using mobile boundaries for grid cells 5-7 (Figure 1), and transfering air between adjacent grid cells as the boundaries move up and down with time of day.

Simulation of turbulent motions above the Amazon forest is complicated. Most of the turbulent energy at canopy height is carried by eddies of size 50-100 m [*Fitzjarrald et al.*, 1988], significantly larger than expected for mechanically generated turbulence. These eddies are likely generated in the active mixed layer, and standard micrometeorological formulations for the turbulent diffusivity (K_z) are probably inapplicable. We choose instead to model turbulent transport by using empirical exchange velocities constrained with observed concentrations and vertical fluxes of O_3, ^{222}Rn, and CO_2. The turbulent mass fluxes are computed as follows:

$$F_{i,k} = V_k(C_{i,k} - C_{i,k+1})N_k \qquad (1)$$

where $F_{i,k}$ (molecules cm^{-2} s^{-1}) is the flux of species i from cell k to cell $k + 1$, V_k is the exchange velocity (cm s^{-1}) between cells k and $k + 1$, $C_{i,k}$ is the mixing ratio (v/v) of species i in cell k, and N_k is the air density (molecules cm^{-3}) at the boundary between cells k and $k + 1$. Our prescription of exchange velocities in the model (Table 1) distinguishes between a "daytime" regime (0900-1600 LT) when turbulence is vigorous, and a "nighttime" regime (1600-0900 LT) when vertical motions are suppressed. Here LT

refers to local (solar) time. Values for V_1, V_2, V_3 are computed on the basis of observed vertical distributions and fluxes of O_3, ^{222}Rn, and CO_2 in the canopy and immediately above [*Trumbore et al.*, this issue; *Fan et al.*, this issue]. The value of V_1 is lower in the daytime than at night, reflecting the greater thermal stability of air near the ground during the day (L. C. B. Molion et al., Micrometeorological dynamics of a terre firme forest in central Amazonia during GTE/ABLE 2B mission, submitted to *Journal of Geophysical Research*, 1989). Values for V_4, V_5, V_6, V_7 are adjusted to fit the observed ^{222}Rn concentrations and O_3 fluxes at canopy top [*Trumbore et al.*, this issue; *Fan et al.*, this issue], as well as the vertical distributions of O_3 in the PBL [*Browell et al.*, this issue; *Gregory et al.*, this issue; *Kirchhoff et al.*, this issue]. The flushing time of the 0-40 m air column in the model (for an inert tracer emitted at the ground) is 1 hour in the daytime and 5 hours at night, in excellent agreement with the values computed by *Trumbore et al.* [this issue] from observations for ^{222}Rn and CO_2. Turbulent exchange at the upper boundary of the model domain (V_7) ventilates the PBL, and entrains into grid cell 7 free tropospheric air assumed to have fixed composition (Table 2). Deposition fluxes to vegetation and to the ground define the lower boundary conditions of the model, and are discussed below.

2.2. *Deposition*

The forest canopy is a sink for oxidants and for water- and lipid-soluble species, which deposit to leaves and soil. Deposition to vegetation is simulated with a resistance-in-series formulation for individual canopy grid cells [*Shreffler*, 1978; *Meyers and Baldocchi*, 1988]. The deposition rate $D_{i,k}$ (molecules cm^{-3} s^{-1}) of species i to vegetation in grid cell k (k=1,3) is given by

$$D_{i,k} = \frac{L_k}{r_{i,k}\Delta Z_k} C_{i,k} \qquad (2)$$

where L_k is the leaf area index of grid cell k (cm^2 leaf area per cm^2 air column, counting only one side of leaf), ΔZ_k is the grid cell thickness (cm), and $r_{i,k}$ (s cm^{-1}) is the leaf resistance to deposition per cm^2 of leaf area (counting only one side of leaf). Following *Meyers and Baldocchi* [1988], we express $r_{i,k}$ as a composite resistance including contributions from leaf-atmosphere boundary (r_{Bk}), stomatal (r_{Sk}), mesophyllic ($r_{Mi,k}$), and cuticular ($r_{Ci,k}$) resistances:

$$r_{i,k} = r_{Bk} + \left[\frac{1}{r_{Ci,k}} + \frac{1}{(\Delta_v/\Delta_i)r_{Sk} + r_{Mi,k}}\right]^{-1} \qquad (3)$$

TABLE 1. Exchange Velocities Between Model Grid Cells

Grid Cell	Exchange Velocity, cm s^{-1}		Top of grid cell, m		Equivalent K_z, cm^{2}s^{-1}	
	0900-1600 LT	1600-0900 LT	Noon	Midnight	Noon	Midnight
1	0.13	0.4	2	2	1.3(2)	4.0(2)
2	2	0.5	20	20	2.8(3)	7.0(2)
3	15	1	30	30	1.5(4)	1.0(3)
4	2	1	40	40	4.7(4)	1.0(3)
5	2	1	500	50	1.5(5)	1.0(3)
6	2	0.05	1500	60	1.5(5)	4.9(3)
7	2	0.05	2000	2000	5.0(4)	4.9(3)

The exchange velocity V_i listed for grid cell i defines the rate of turbulent mass exchange between grid cells i and i+1, as computed from (1). For completeness, we also list the "equivalent" turbulent diffusivity at the top of grid cell i, $K_{z,i} = V_i \Delta Z_i$, where ΔZ_i is the distance between the centerpoints of grid cells i and i+1. However $K_{z,i}$ is not truly equivalent to V_i because individual grid cells are assumed well-mixed. Read 1.3(2) as 1.3 x 10^{-2}.

TABLE 2. Upper Boundary Model Concentrations at 2000 m Altitude

Species	Concentration, ppb	Reference
Isoprene	0.1	*Rasmussen and Khalil* [1988]
Acetone	0.8	a
CO	80	*Harriss et al.* [this issue (b)]
NO	0.005	*A.L. Torres and K.R. Hooks* (submitted manuscript, 1989)
NO_2	0.005	b
PAN	0.02	*Singh et al.* [this issue]
HNO_3	0.2	b
RNO_3	0.01	b,c
H_2O_2	2.5	*Logan et al.* [1981]
CH_3OOH	2	*Logan et al.* [1981]
$ROOH^d$	0.01	b
O_3	18	*Browell et al.* [this issue]

[a] Estimated biogenic continental background (D. Pierotti and S.C. Wofsy, Acetone, acetaldehyde, and other carbonyls in the atmosphere, submitted to *Journal of Geophysical Research, 1989.*)

[b] Assumed.

[c] A concentration of 1 ppb is assumed in the sensitivity calculation with exogenous organic nitrates (section 6).

[d] Other than CH_3OOH.

where $\Delta_v = 0.22$ cm^2 s^{-1} and Δ_i are the molecular diffusivities in air of water vapor and species i, respectively. We assume a total leaf area index $L = 7$ for the Amazon forest canopy, based on the data of *Shuttleworth et al.* [1984] as discussed by *Fan et al.* [this issue]. This leaf area index represents a sum of contributions L_k from each grid cell in the canopy layer:

$$L = \sum_1^3 L_k \qquad (4)$$

with $L_1 = 1$, $L_2 = 2$, and $L_3 = 4$ [*Fan et al.*, this issue].

The boundary and stomatal leaf resistances used in the model (Table 3) are the average values measured at the ABLE 2B forest site by *Roberts et al.* [1990], as a function of time of day and altitude. Inspection of Table 3 indicates that the leaf-atmosphere boundary resistances are always small compared to the stomatal resistances, and therefore have little influence on deposition rates. The stomatal resistances are lowest in the upper canopy, and highest near the ground, presumably because of stomatal response to low light levels but also possibly because of differences in the species present at various altitudes within the canopy. In the middle and upper canopy the stomatal resistances are lowest in mid-morning, and then increase progressively over the rest of the day. This diurnal pattern appears to reflect the combined effects of water stress and insolation [*Roberts et al.*, 1990].

Following *Wesely* [1989], we assume zero mesophyllic resistance for oxidants (O_3, peroxyacylnitrates, peroxides, NO_2) and for water-soluble species with effective Henry's Law constants larger than 10^3 moles l^{-1} atm^{-1} at pH 7 (e.g., HNO_3, HNO_2, CH_2O, dicarbonyls). Zero mesophyllic resistance is also assumed for isoprene (which is lipid soluble) and for organic nitrates (in order to simulate the downward flux of NO_y observed by *Bakwin et al.* [this issue (a)]. All other species are taken to have infinite mesophyllic resistance, i.e., they are not removed at the stomata.

At night the stomata are closed, and deposition to the leaves proceeds at the outer (cuticular) surfaces only. Cuticular resistances to deposition are high except for oxidants and for highly water-soluble species [*Wesely*, 1989]. We adopt $r_C = 10$ s cm^{-1} for O_3, which gives a good fit to the observed nighttime fluxes of O_3 [*Fan et al.*, this issue]. We similarly adopt $r_C = 10$ s cm^{-1} for other oxidants (peroxyacylnitrates, peroxides, NO_2), and also for

HNO_3 and organic nitrates. Other depositing species (i.e., other species with $r_M = 0$) are assumed to be removed with $r_C = 100$ s cm^{-1}, on the basis of data for water vapor [*Jones*, 1983].

Deposition to the ground provides an additional sink for species in grid cell 1, with flux G_i (molecules cm^{-2} s^{-1}):

$$G_i = \frac{C_{i,1}}{r_{Gi}} \qquad (5)$$

Following *Wesely* [1989] we assume $r_G = 2$ s cm^{-1} for all oxidants (and also for HNO_3 and organic nitrates), and $r_G = 5$ s cm^{-1} for other depositing species.

TABLE 3. Leaf Resistances for Deposition to Vegetation

	Time of Day, LT	Grid Cell 1	2	3
Altitude range (m)		0-2	2-20	20-30
Boundary resistance		1.7	0.53	0.37
Stomatal resistance	0600	4.3	4.3	2.8
	0700	4.3	4.3	2.1
	0800	4.3	3.4	1.9
	0900	4.3	1.9	1.7
	1000	4.3	2.5	1.9
	1100	4.3	2.8	1.9
	1200	4.3	2.8	2.1
	1300	4.3	3.4	2.1
	1400	4.3	4.3	2.5
	1500	4.3	5.7	2.8
	1600	8.6	8.6	4.3
	1700	8.6	8.6	8.6
	1800	8.6	8.6	8.6

Resistance units are s cm^{-1} per cm^2 of leaf area, counting only one side of leaf. The resistances are taken from the average values reported by *Roberts et al.* [1990] at the ABLE 2B forest site. The stomatal resistances as given by *Roberts et al.* [1990] are multiplied by $6/7 = 0.86$, as these authors made their measurements mainly on the lower surfaces of the leaves, and reported that stomatal areas on the upper surfaces of the leaves were typically 6 times smaller than on the lower surfaces. Stomatal resistances at night are assumed infinitely large.

Rainfall scavenges water-soluble species efficiently. Observed precipitation fluxes of sulfate and organic acids during ABLE 2B indicate a time constant of 1 day for wet removal from the PBL [*Andreae et al.*, this issue (*a*)]. We use this time constant in the model to simulate wet deposition of species with effective Henry's law constants larger than 10^3 moles l^{-1} atm^{-1} at pH 5, including organic peroxides (for which solubility constants are largely unknown). Less soluble species (e.g., NO$_x$, PAN, organic nitrates) are not removed by wet deposition.

2.3. Biogenic Emissions

The soil in grid cell 1 is viewed as a constant source of NO and CO to the atmosphere. We adopt an emission flux of 8.7 x 10^9 molecules cm^{-2} s^{-1} for NO, which is the mean value measured for clay soils during ABLE 2B [*Bakwin et al.*, this issue (*b*)]. A CO emission flux of 3 x 10^{11} molecules cm^{-2} s^{-1} is assumed, on the basis of flux estimates at canopy top by *Kirchhoff and Marinho* [this issue]. The CO fluxes observed by *Kirchhoff and Marinho* [this issue] could possibly reflect emissions from the forest vegetation, rather than from soil [*Seiler*, 1978]; however, the precise origin of this biogenic CO is of no consequence for our model purposes.

Isoprene provides a major sink for OH over the Amazon forest [*Zimmerman et al.*, 1988]. We assume that the isoprene emission flux from the forest vegetation depends on the local air temperature and photosynthetically active radiation (PAR). The dependence on temperature is taken from *Lamb et al.* [1987], and the dependence on PAR is taken from *Tingey et al.* [1979]. The isoprene emission flux per unit area of leaf, ϕ (molecules cm^{-2} leaf s^{-1}), is computed as follows:

$$\phi = \phi_o \, e^{\zeta(T-298)} \exp\left[\frac{a}{1+e^{-b(I-c)}}\right] \qquad (6)$$

where $\zeta = 0.1$ [*Lamb et al.*, 1987], $a = 10.2$, $b = 0.0064$, $c = 11$ [*Tingey et al.*, 1979], T is the local air temperature (K), I is the local PAR (microeinsteins m^{-2} s^{-1}), and $\phi_o = 1$ x 10^7 molecules cm^{-2} leaf s^{-1} is a parameter adjusted in the model to provide a reasonable simulation of atmospheric isoprene concentrations. For a leaf at 298 K exposed to full sun, the isoprene emission flux calculated from (6) is 2.7 x 10^{11} molecules cm^{-2} leaf s^{-1}. The rate of isoprene emission in grid cell k, E_k (molecules cm^{-3} s^{-1}), scales linearly to the vegetation density $L_k/\Delta Z_k$, and is computed as follows:

$$E_k = \phi_o \frac{L_k}{\Delta Z_k} \, e^{\zeta(T_k-298)} \frac{1}{z_t-z_b} \int_{z_b}^{z_t} \exp\left[\frac{a}{1+e^{-b(I(z)-c)}}\right]dz \qquad (7)$$

where z_b and z_t are the altitudes at the bottom and at the top of grid cell k, respectively.

Values for T_k range from 295 K in grid cell 1 in early morning to 302 K in grid cell 3 at midday [*Fitzjarrald and Moore*, this issue; *Fitzjarrald et al.*, this issue]. This temperature range produces only a factor of 2 variation in isoprene emission rates. Light intensity plays a more important role in regulating isoprene emissions from the Amazon forest. The PAR at altitude z is computed by assuming that vegetation behaves as a gray absorber:

$$I(z) = I_T \, e^{-\tau(z)/\cos\theta} \qquad 0 \le z \le 30 \text{ m} \qquad (8)$$

where I_T is the PAR at the top of the canopy (30-m altitude), $\tau(z)$

is the overhead canopy optical depth at altitude z, and θ is the solar zenith angle. We compute $\tau(z)$ as follows:

$$\tau(z) = k_{ex} l(z) \qquad 0 \le z \le 30 \text{ m} \qquad (9)$$

where k_{ex} is the coefficient for light extinction by vegetation normalized to the leaf area index, and $l(z)$ is the leaf area index from altitude z to the top of the canopy. A constant value $k_{ex} = 0.5$ is assumed, corresponding to a uniform angular distribution of leaf orientations [*Verstraete*, 1987]. Values for I_T are taken from the mean hourly solar irradiances for April-May measured at the Embrapa station 2 km from the ABLE 2B forest site (O. M. R. Cabral, personal communication, 1988). Following *Parsons et al.* [1977], we assume that 50% of the solar radiation is photosynthetically active, and apply a conversion factor 1 W = 4.60 microeinsteins s^{-1} to convert the resulting PAR energy flux to a photon flux. The values of I_T computed in this manner peak at 1270 microeinsteins m^{-2} s^{-1} at noon, and show little asymmetry about the noontime peak.

The simulated flux of isoprene at canopy top is shown in Figure 2 as a function of time of day. This flux represents the sum of emissions from each canopy grid cell, partly balanced by deposition. The upper canopy grid cell (20-30 m) accounts for 98% of total isoprene emission by the forest, mainly because light attenuation inhibits emission from leaves deeper in the canopy. Vegetative emissions of acetaldehyde, organic acids, and reduced sulfur species are scaled to isoprene emission, with a scaling factor of 2% for acetaldehyde [D. Pierotti and S. C. Wofsy, Acetone, acetaldehyde, and other carbonyls in the atmosphere, submitted to *Journal of Geophysical Research*, 1990], and scaling factors for organic acids and sulfur species adjusted to provide simulated concentrations in harmony with observations [*Talbot et al.*, this issue (*b*); *Andreae et al.*, this issue (*b*)]. The daily mean fluxes at canopy top of species emitted by vegetation are listed in Table 4. The flux of acetaldehyde relative to isoprene in Table 4 is higher than would be expected from the scaling of emissions; this result reflects mainly the assumed lack of acetaldehyde deposition to vegetation.

Emissions of terpenes are not included in the model. The dry season hydrocarbon measurements of *Zimmerman et al.* [1988] indicate that the total concentration of terpenes over the forest is less than 10% of the isoprene concentration on a molar basis, therefore terpenes should have little influence on photochemistry. However, *Zimmerman et al.* [1988] observed significant concentrations of
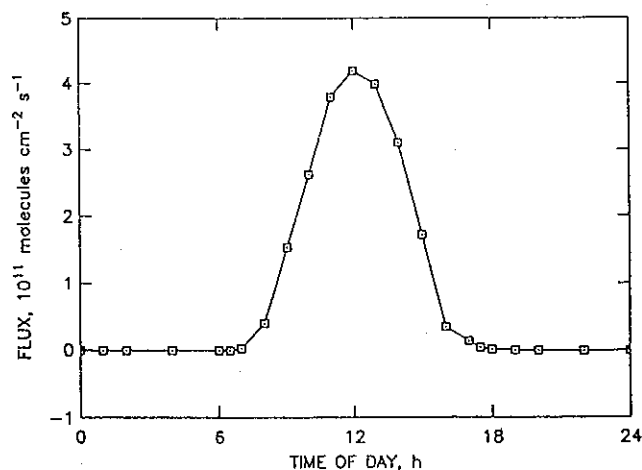
Fig. 2. Vertical flux of isoprene at 40 m in the model, as a function of time of day. Positive values indicate an upward flux.

TABLE 4. Upward Fluxes at Canopy Top of Species
Emitted by Vegetation

Species	Flux, molecules $cm^{-2} s^{-1}$
Isoprene	9.1 (10)
Acetaldehyde	4.0 (9)
Formic acid	4.4 (9)
Acetic acid	3.7 (9)
Pyruvic acid	2.8 (8)
H_2S	1.4 (9)
$(CH_3)_2S$	3.4 (8)
CH_3SH	1.7 (8)

Daily mean fluxes at 30 m (canopy top), representing a balance
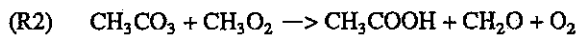between vegetative emissions and dry deposition. Read 9.1 (10) as
9.1×10^{10}.

other nonmethane hydrocarbons (NMHCs) including alkanes, alk-
enes, and aromatic compounds. Biomass burning appeared to be a
major source of these NMHCs, and such a source would be re-
duced considerably in the wet season. Unfortunately, no NMHC
data are available for the wet season. In our standard model calcu-
lation, we neglect all NMHCs except for those listed in Table 4
and their decomposition products. A sensitivity calculation (sec-
tion 9) will examine the effect of adding other NMHCs at the dry
season levels reported by *Zimmerman et al.* [1988]. As we will
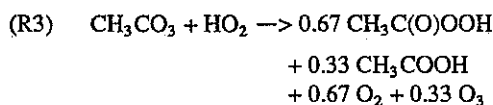see, the effect is small.

2.4. Chemical Mechanism

Photochemistry is simulated with the detailed mechanism of
Lurmann et al. [1986], modified for low-NO_x conditions as
described by *Jacob and Wofsy* [1988]. Rate constants and
stoichiometries for some reactions of CH_3O_2 and CH_3CO_3 have
been updated on the basis of recent kinetic data [*Moortgaat et al.,*
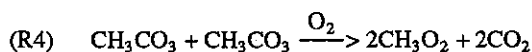1989*ab*]:

(R1) $CH_3CO_3 + CH_3O_2 \xrightarrow{O_2} CH_3O_2 + CH_2O + HO_2 + CO_2$
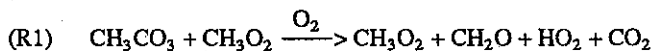
$$k_1 = 1.8 \times 10^{-9} \ e^{-1800/T} \ cm^3 \ molecule^{-1} \ s^{-1}$$

(R2) $CH_3CO_3 + CH_3O_2 \longrightarrow CH_3COOH + CH_2O + O_2$

$$k_2 = 4.1 \times 10^{-15} \ e^{(2100/T)} \ cm^3 \ molecule^{-1} \ s^{-1}$$

(R3) $CH_3CO_3 + HO_2 \longrightarrow 0.67 \ CH_3C(O)OOH$
$$+ 0.33 \ CH_3COOH$$
$$+ 0.67 \ O_2 + 0.33 \ O_3$$

$$k_3 = 4.3 \times 10^{-13} \ e^{(1040/T)} \ cm^3 \ molecule^{-1} \ s^{-1}$$

(R4) $CH_3CO_3 + CH_3CO_3 \xrightarrow{O_2} 2CH_3O_2 + 2CO_2$

$$k_4 = 2.8 \times 10^{-12} \ e^{(530/T)} \ cm^3 \ molecule^{-1} \ s^{-1}$$

Atmospheric oxidation of hydrocarbons in the model yields a
variety of organic peroxy and peroxyacyl radicals [*Lurmann et al.,*
1986]. We label these radicals collectively as one chemical fami-
ly, RO_2, and the peroxyacyl radicals collectively as RCO_3, a sub-
family of RO_2. Kinetic data for RO_2 radicals are largely limited
to the smaller species CH_3O_2 and CH_3CO_3. The principal atmos-
pheric sinks for CH_3O_2 are the reactions with NO and HO_2, and

the self-reaction. Reaction with O_3 is negligibly slow [*Atkinsor
and Lloyd,* 1984]. The CH_3CO_3 radical is consumed by similar
reactions as for CH_3O_2, and reacts in addition with NO_2 to pro-
duce PAN. Following *Lurmann et al.* [1986], we assume that the
rate constants for reactions of all RO_2 radicals with NO and HO_2
are the same as for CH_3O_2. However RCO_3 radicals react with
HO_2 and NO_2 at the same rate as CH_3CO_3. The RO_2-RO_2 reac-
tions involving $>C_1$ RO_2 radicals (RO_2 radicals other than CH_3O_2
or CH_3CO_3) are assumed negligible. Stoichiometries and rate
constants for the RO_2 and RCO_3 reactions are as follows:

(R5) $RO_2 + NO \xrightarrow{O_2, multisteps} \alpha R'COR'' + \beta NO_2$
$$+ (1 - \beta)RNO_3$$
$$+ \gamma HO_2 + \delta R'''O_2$$
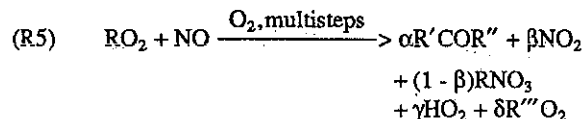
$$k_5 = 4.2 \times 10^{-12} \ e^{180/T} \ cm^3 \ molecule^{-1} \ s^{-1}$$

(R6) $RO_2 + HO_2 \longrightarrow ROOH + O_2$

$$k_6 = 4.3 \times 10^{-13} \ e^{(1040/T)} \ cm^3 \ molecule^{-1} \ s^{-1}$$
(for RCO_3 radicals)
$$k_6 = 4.5 \times 10^{-12} \ cm^3 \ molecule^{-1} \ s^{-1}$$
(for non-RCO_3 radicals)

(R7) $RCO_3 + NO_2 \underset{b}{\overset{f}{\rightleftharpoons}} RPAN$

$$k_{7f} = 4.7 \times 10^{-12} \ cm^3 \ molecule^{-1} \ s^{-1}$$
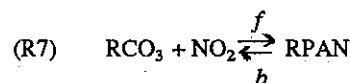$$k_{7b} = 1.95 \times 10^{16} \ e^{-13543/T} \ cm^3 \ molecule^{-1} \ s^{-1}$$

where $R'COR''$, RNO_3, $ROOH$, and RPAN represent carbonyls,
organic nitrates, organic peroxides, and peroxyacylnitrates,
respectively. The product yields in (R5) depend on the nature of
the RO_2 radical; for the RO_2 radicals arising from isoprene
decomposition the ranges are $\alpha = 0.9$-1.8 , $\beta = 0.9$-1, $\gamma = 0.3$-1,
and $\delta = 0$-0.6 [*Lloyd et al.,* 1983]. All RPAN species are assumed
to decompose thermally at the same rate as PAN [*Lurmann et al.,*
1986]. Organic peroxides produced by (R6) are removed in the
model by wet and dry deposition; they may also react with OH, or
photolyze, with lifetimes of a few days against either of these
chemical sinks [*Jacob and Wofsy,* 1988]. Organic nitrates are as-
sumed unreactive in the atmosphere, but they are removed by dry
deposition.

The UV radiation intensities are computed with a six-stream al-
gorithm for the Rayleigh atmosphere [*Logan et al.,* 1981], assum-
ing an O_3 column of 7.1×10^{18} molecules $cm^{-2} \ s^{-1}$ [*Kirchhoff et
al.,* this issue], 30% opaque cloud cover above 2000 m [*Menzel et
al.,* this issue], and a Lambertian reflectivity of 0.1 at canopy top.
Scattering of radiation by clouds within the PBL is ignored. Light
extinction by aerosols is assumed to provide 0.1 total vertical opti-
cal depth at 310 nm, varying inversely with wavelength [*Logan et
al.,* 1981]. Radiation intensities within the canopy are corrected
for light extinction by vegetation following (8). Temperatures
range from 302 K near canopy top at midday to 295 K in the upper
PBL, and partial pressures of water vapor range from 17 mbar in
the upper PBL to 30 mbar near the ground at night, based on ob-
servations.

2.5. Computational Procedure

The chemical evolution of the atmosphere is computed by solv-
ing a system of coupled differential equations expressing the
changes in the concentrations of species in all grid cells as a result

f chemistry, emissions, deposition, and vertical transport. The solution is obtained by an implicit finite difference method [Richtmeyer, 1957] with time steps ranging from 30 min in the day to 2 hours at night. At the end of each time step the photolysis rates and the emission fluxes from vegetation are updated; the mobile grid cell boundaries are adjusted vertically, and changes in species concentrations due to entrainment are computed. We established in test simulations that these time steps are sufficiently small to ensure stable and accurate solutions.

The model simulation is conducted over 3 diurnal cycles, starting from 0000 LT. The composition of the PBL is initialized at the beginning of the simulation with free tropospheric air, i.e., the upper boundary conditions in Table 2 are taken as initial conditions. This initialization is intended to simulate the passage of a major meteorological disturbance, when air from the free troposphere is rapidly mixed with the PBL. As the simulation progresses, the concentrations of the various species increase or decrease from the initial values, approaching eventually a steady state between model sources and sinks. For a long-lived species emitted by the forest, and removed by ventilation through the top of the model domain (e.g., CO), the characteristic time required to reach steady state in the model is about 7 days; a similar time is required for a species transported to the PBL from the free troposphere, and removed by deposition to the canopy (e.g., O_3). According to data for ^{222}Rn (E. B. Pereira et al., unpublished manuscript, 1989), the residence time of air in the PBL over the Amazon Basin is roughly 3 days. Therefore we do not expect the atmosphere to reach a steady state as described by the model sources and sinks. Nevertheless, we find that changes in the simulated atmospheric composition between model days 2 and 3 are relatively small; the 24-hour average PBL concentrations of O_3, NO_x, isoprene, and PAN change by -9%, +9%, +12%, and +25%, respectively (the increase is greatest for PAN as it reflects the combined increases of NO_x and isoprene concentrations). We focus on the results from model day 3 as representative of the general chemical behavior of the PBL, subject to rapid exchange with the free troposphere or with air from outside the Basin every 2 or 3 days. Except if indicated otherwise, all model results presented below are from model day 3.

3. CHEMICAL BUDGETS IN THE CANOPY

Figure 3 shows mean O_3 concentrations observed within the canopy during ABLE 2B [Bakwin et al., this issue (a)] (right panel) as well as computed values (left panel). Reasonable agree-

ment is found throughout the day, reflecting in part the adjustment of exchange velocities in the model (cf. section 2.1). The concentrations of O_3 within the canopy are regulated largely by supply from aloft and deposition to vegetation, as shown in Table 5. Photochemical production provides a small additional source in the daytime (150 ppt h^{-1} at noon), and reaction with NO provides a small additional sink at night (260 ppt h^{-1} at midnight). The simulated vertical O_3 fluxes at 40 m are in good agreement with the eddy correlation flux measurements of Fan et al. [this issue] (Figure 4). Ozone fluxes are much larger in the daytime than at night, reflecting both the opening of the stomata in the daytime and the increased turbulence at canopy top; further discussion of these factors is given by Fan et al. [this issue]. A gradual decrease in the O_3 flux is found between mid-morning and afternoon, both in the model and in the observations. This asymmetry appears to follow the increase in stomatal resistances over the course of the day (Table 3).

Simulated NO concentrations within the canopy are compared in Figure 5 to the mean observations from ABLE 2B [Bakwin et al., this issue (a)]. Model results are in general harmony with these observations. The nighttime budget of NO in the model (Table 5) represents largely a balance between soil emission and reaction with O_3. Accumulation of NO in the canopy air column (33 ppt h^{-1} at midnight) is only a small term in the budget, in agreement with data from Bakwin et al. [this issue (b)], which indicate an average nighttime NO accumulation rate of 15 ± 110 ppt h^{-1} in the 0-41 m air column.

Nighttime oxidation of NO to NO_2 in the model is followed by deposition of NO_2 to vegetation, which limits the fraction of NO_x emitted by soil that is exported to the PBL (Table 5). The deposition of NO_2 in the model follows from our assumption of a low cuticular resistance for uptake of NO_2 by vegetation ($r_C = 10$ s cm^{-1}). We find that efficient nighttime uptake of NO_2 by vegetation is necessary to explain the NO_y concentrations of 300-600 ppt observed at 19-39 m by Bakwin et al. [this issue (a)], as these observations provide a constraint on the maximum accumulation of NO_x in the nighttime mixed layer. If NO_x were assumed not to deposit at night then the NO_x concentration simulated by the model at 30-40 m would exceed 1 ppb at midnight, and 2 ppb at dawn, inconsistent with the NO_y data. Obviously the NO_x concentrations predicted by the model are dependent on the simulation of transport; the inconsistency with the NO_y data would vanish if the ventilation rate of the nighttime mixed layer in the model were increased by a factor 3. However such an increase would imply a flushing time of less than 2 hours for the 0-40 m air
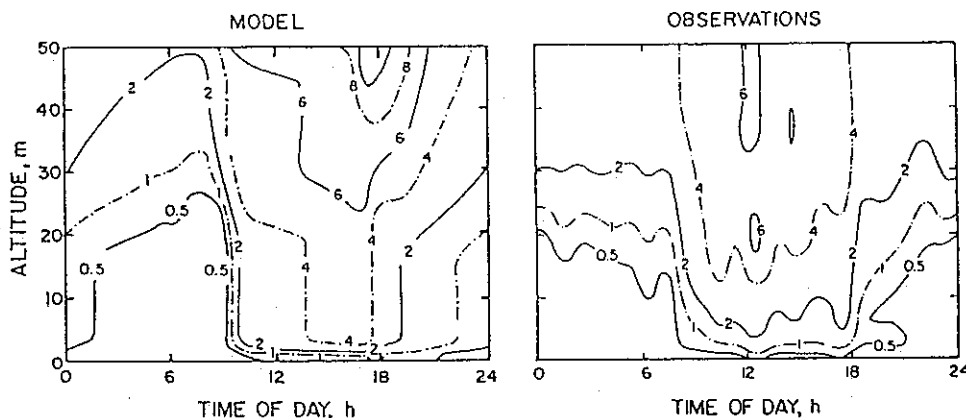

Fig. 3. Concentrations of O_3 (ppb) between 0 and 50 m, as a function of time of day. Model results (left panel) are compared to the observations of Bakwin et al. [this issue (a)] (right panel).

TABLE 5. Budgets of O_3, NO, and NO_x in the 0-40 m air column

	O_3		NO		NO_x	
	Noon	Midnight	Noon	Midnight	Noon	Midnight
Concentration, ppt	4420	1250	153	240	264	556
Sources and sinks, ppt h^{-1}						
Soil emission			+330	+330	+330	+330
Flux at 40 m	+9450	+710	-44	-19	-92	-31
Deposition	-9190	-740			-275	-252
NO + O_3	-430	-260	-429	-261		
HO_2+NO			-189	-8		
RO_2+NO			-270	-9		
NO_2 + hv	+580		+583			
PAN decomposition					<1	<1
RPAN decomposition					+2	<1
Accumulation, ppt h^{-1}	+410	-290	-19	+33	-35	+47

Model results averaged over the 0-40 m air column.

column, while the ^{222}Rn data of *Trumbore et al.* [this issue] indicate a mean flushing time of 5.5 hours at night. Also, higher ventilation rates in the model would produce excessive nighttime O_3 fluxes, and would require very low cuticular resistances for O_3 deposition (r_C = 2.5 - 5 s cm^{-1}) in order to simulate the O_3 levels observed in the canopy. It appears therefore that substantial nighttime loss of NO_x must take place inside the canopy. Deposition of NO_2, as simulated by the model, is a likely mechanism to explain this loss.

The observed NO concentrations show a pronounced surge shortly after sunrise (Figure 5). This surge is well simulated in the model, where it is due to photolysis of NO_2 accumulated in the canopy over the course of the night. Following the surge the NO concentrations drop sharply, as the onset of daytime turbulence ventilates NO_x from the canopy. The daytime budget of NO_x in the canopy represents a balance between soil emission of NO, deposition of NO_2 to vegetation, and ventilation to the PBL (Table 5), similarly to the nighttime budget. Ventilation and deposition rates are both enhanced in the daytime, and deposition remains the dominant term balancing soil emissions. The lower NO_x concentrations in the canopy in the daytime than at night can thus be attributed primarily to stomatal opening, rather than to enhanced turbulence.
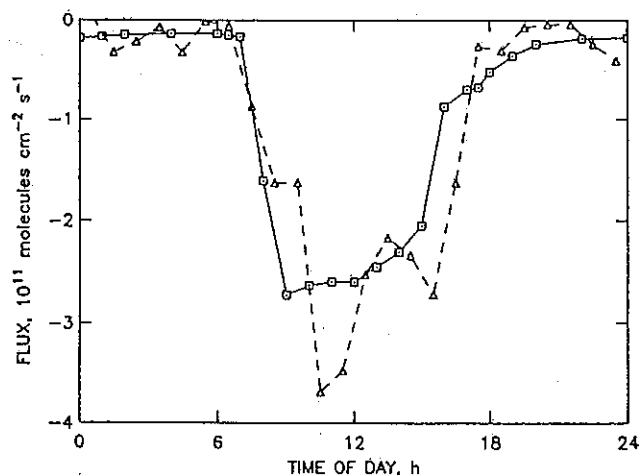

Fig. 4. Vertical flux of O_3 at canopy top, as a function of time of day. Model results at 40 m (solid line) are compared to the eddy correlation measurements at 39 m of *Fan et al.* [this issue] (dashed line). Negative values indicate a downward flux.

Simulated upward fluxes of NO_x at 40 m altitude are shown in Figure 6 as a function of time of day. These can be compared to the soil emission flux of NO, 8.7 x 10^9 molecules cm^{-2} s^{-1}. On a 24-hour average basis only 19% of NO_x emitted by soil is exported to the PBL; the balance is removed by deposition to the canopy. Export is strongest in mid-morning, when NO_x accumulated in the canopy over the previous night is ventilated to the growing mixed layer. During the remainder of the daytime hours the export of NO_x represents about 25% of the soil emission rate, declining to about 13% at night.

4. HYDROCARBONS

Detailed isoprene concentrations measured during ABLE 2B are not available, but a preliminary report [*Dalluge et al.*, 1987] indicates that concentrations were similar to those observed by *Rasmussen and Khalil* [1988] during the dry season ABLE 2A expedition. Model results (Figure 7) are generally consistent with the aircraft observations of *Rasmussen and Khalil* [1988], although simulated concentrations near the surface are somewhat higher. The average model chemical lifetime of isoprene in the daytime PBL is 6.4 hours; reaction with OH contributes 92% of the sink and reaction with O_3 contributes most of the balance. At midday, the lifetime ranges from 21 hours at canopy top to 1.5 hours in the upper PBL, reflecting the vertical distribution of OH (cf. section 7). The long lifetime of isoprene near the surface allows it to be transported to relatively high altitudes, where it is then rapidly oxidized. Chemical removal of isoprene at night is slow because of the low concentration of NO_3 [cf. *Jacob and Wofsy*, 1988].

Average concentrations of NMHCs in the PBL are listed in Table 6. The NMHCs are produced mainly by photochemical decomposition of isoprene, except for those species emitted directly by vegetation (Table 4). The low concentrations of NO in the PBL favor the formation of organic peroxides, which may be removed by wet and dry deposition (69% of the organic peroxide sink in the model) or recycled into the hydrocarbon pool by photolysis and reaction with OH.

Oxidation of isoprene contributes 91% of the simulated CH_2O over the forest. The simulated CH_2O concentration of 0.5 ppb is higher than observations in marine air ($\approx$ 0.2 ppb [*Lowe and Schmidt*, 1983]), but lower than observations in rural air at northern mid-latitudes (1-2 ppb [*Neitzert and Seiler*, 1981; *Snider and Dawson*, 1985]). It appears that oxidation of isoprene can enhance
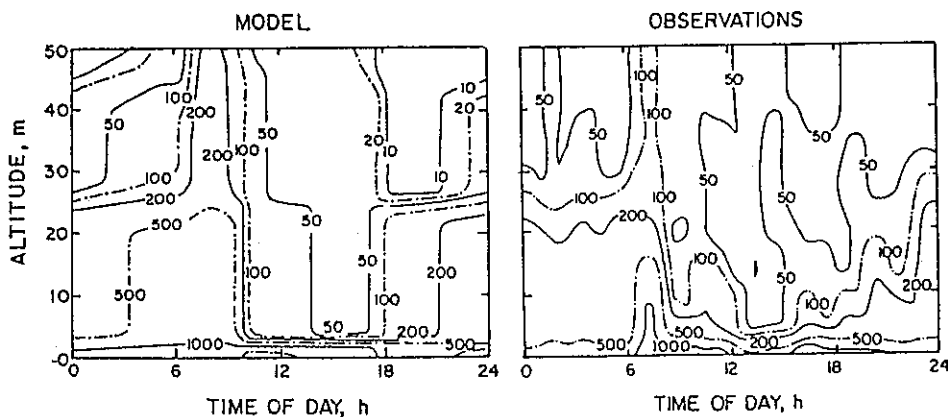
MODEL   OBSERVATIONS

Fig. 5. Concentrations of NO (ppt) between 0 and 50 m, as a function of time of day. Model results (left panel) are compared to the observations of *Bakwin et al.* [this issue *(a)*] (right panel).
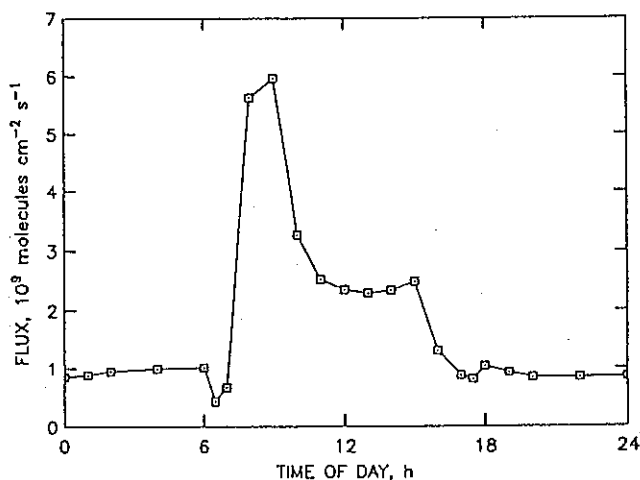
significantly the CH_2O concentration in remote continental air as compared to marine air. At northern mid-latitudes, oxidation of anthropogenic NMHCs provides probably a major additional source of CH_2O [*Kasting and Singh*, 1986].

Photolysis of methylglyoxal produced from decomposition of isoprene constitutes in the model the major source of the CH_3CO_3 radical (Table 7). Two other important sources are the oxidation of acetaldehyde by OH, and the $RO_2 + NO$ reaction where RO_2 is a peroxy radical generated in the oxidation of methylvinylketone by OH [*Lloyd et al.*, 1983]. High production rates for CH_3CO_3 displace the NO_2/PAN equilibrium towards PAN, inhibiting the decomposition of PAN to NO_x. As we will see below, the production of CH_3CO_3 radicals in the model is sufficiently high to lead to net formation of PAN at midday in the lower PBL.

5. CARBON MONOXIDE

Carbon monoxide accumulates progressively in the PBL over the course of the simulation. Starting from the free troposphere concentration of 80 ppb assumed as initial condition, the mean CO

Fig. 6. Vertical flux of NO_x at 40 m in the model, as a function of time of day. Positive values indicate an upward flux.
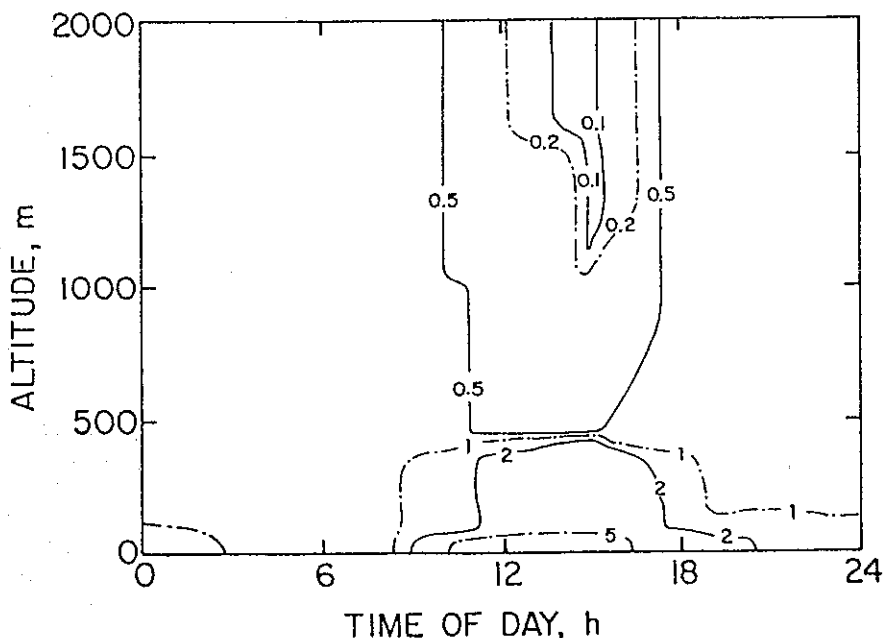
Fig. 7. Simulated concentrations of isoprene (ppb) in the PBL, as a function of altitude and time of day.

concentration in the PBL rises to 84.1, 88.0, and 91.2 ppb at the end of model days 1, 2, and 3, respectively. *Harriss et al* [this issue *(b)*] observed 5-10 ppb enhancements of CO concentration in the PBL relative to the free troposphere during ABLE 2B; model results are consistent with these observations. The net accumulation of CO in the PBL over the course of model day 3 is 3.2 ppb d^{-1}, reflecting sources from direct emission (5.9 ppb d^{-1}) and secondary production (0.8 ppb d^{-1}), and sinks from ventilation to the free troposphere (2.9 ppb d^{-1}) and reaction with OH (0.6 ppb d^{-1}). The CO concentration would reach 100 ppb after about 7 model days, but it is unlikely that the PBL could evolve over such a long period during the wet season without a major storm disturbance or influx of oceanic air [*Scala et al.*, this issue; E. B. Pereira et al., unpublished manuscript, 1989].

TABLE 6. Concentrations of Biogenic Hydrocarbons

Species	Concentration, ppt
Isoprene	831
Methylhydroperoxide	474
Organic peroxides*	472
Formaldehyde	472
Methylvinylketone	422
Methacrolein	370
Formic acid	156
Acetic acid	153
$C_{3,5}$-aldehydes[†]	132
Acetaldehyde	129
Hydroxyacetaldehyde	36
RNO_3[‡]	32
Methacrylic acid	27
RO_2	20
RPAN	12
Methylglyoxal	9
$(CH_3)_2S$	7
Pyruvic acid	5
PAN	5
CH_3SH	3

Daily mean model concentrations in the PBL air column (30-2000 m).

* Other than methylhydroperoxide, which is listed separately.

† Other than methacrolein, which is listed separately.

‡ Biogenic organic nitrates other than peroxyacylnitrates, which are listed separately as PAN and RPAN. In the simulation with exogenous organic nitrates the daily mean RNO_3 concentration in the PBL is 776 ppt (cf. Table 8).

TABLE 7. Sources of the Peroxyacetyl Radical

	CH_3CO_3 Production Rate, ppt h^{-1}
Methylglyoxal + *hv*	5.4
Acetaldehyde + OH	2.1
MRO_2 + NO	2.0
Acetone + hv	0.7
ARO_2 + HO_2	0.4
Methylvinylketone + O_3	0.3
Peroxyacetic acid + OH	0.3
PAN decomposition	0.1
Miscellaneous	0.1
Total source	11.4

Daily mean model rates in the PBL air column (30-2000 m). MRO_2 and ARO_2 are RO_2 radicals produced from the methylvinylketone + OH and acetone + OH reactions, respectively.

Direct emission from the forest accounts for 88% of the total PBL source of CO in the model. Production of CO from oxidation of isoprene is small in comparison. Although isoprene emission is an important source of organic carbon to the PBL (9.0 ppb C d^{-1}), oxidation of this carbon to CO is inefficient because of the low photochemical reactivity of the atmosphere, and because hydrocarbon intermediates (organic peroxides, CH_2O) are removed efficiently by wet deposition. An inventory of isoprene carbon on model day 3 indicates that 39% of this carbon is deposited to the forest as organic peroxides and CH_2O; accumulation of hydrocarbon intermediates in the PBL and ventilation to the free troposphere account for 15% and 13% of the carbon, respectively, while 23% is oxidized directly to CO_2, bypassing CO. Only 10% of the isoprene carbon is oxidized to CO within the PBL.

Our predicted CO yield from oxidation of isoprene is much lower than the value of 60-80% previously derived by *Zimmerman et al.* [1978] from a photochemical mechanism for isoprene oxidation. Part of the reason is that we restrict our analysis to CO production within the PBL; however, even without such a restriction our CO yield would still be less than 30%. *Zimmerman et al.* [1978] assumed that NO was present at sufficiently high levels to provide the only significant RO_2 sink, and they did not consider deposition of hydrocarbon intermediates. If we made the same assumptions in our mechanism we would obtain a 60% CO yield from complete isoprene oxidation, consistent with the results of *Zimmerman et al.* [1978]; inclusion of deposition would lower the CO yield to 44%, mainly because of wet deposition of CH_2O. The yield is lowered further by reactions of RO_2 with HO_2, which in the model provide about half (48%) of the RO_2 sink over the Amazon forest. The organic peroxides produced by the RO_2 + HO_2 reactions are primarily removed by wet deposition; they may also photolyze or react with OH to produce $C_{3,5}$ aldehydes, which partially undergo direct oxidation to CO_2 upon further reaction with OH. Obviously, our assessment of the CO yield from isoprene oxidation at low NO_x levels suffers from poor understanding of the atmospheric chemistry of organic peroxides.

6. REACTIVE NITROGEN

Model results for concentrations of NO and PAN are shown in Figure 8 as a function of altitude and time of day. A. L. Torres and K. R. Hooks (submitted manuscript, 1989) observed NO concentrations of 12 ± 7 ppt in the lower PBL (up to 300 m) and 6 ± 3 ppt in the upper PBL (300-2000 m), in harmony with model results. The mid-morning surge in NO concentrations is due to ventilation of NO_x accumulated in the canopy the previous night. Results for PAN are consistent with the observations of *Singh et al.* [this issue], who found daytime PBL concentrations ranging from 5 to 20 ppt. The simulated PAN concentrations are higher in the daytime than at night because downward transport from the free troposphere is faster, and because PAN decomposition in the daytime is inhibited by CH_3CO_3 radicals produced from isoprene oxidation. A weak maximum in PAN concentrations is predicted in the lower PBL at midday when the abundant supply of CH_3CO_3 radicals leads to net conversion of NO_x to PAN.

The main source of NO_x to the PBL is emission from soils, as shown in Table 8. Decomposition of PAN provides only a small source in comparison. The downward flux of PAN from the free troposphere would need to be 10 times greater than simulated in order to provide a source of reactive nitrogen to the PBL comparable to the upward flux of NO_x from the canopy; such rapid vertical transport would however be seriously inconsistent with the observed vertical distributions and fluxes of O_3. Conceivably, PAN
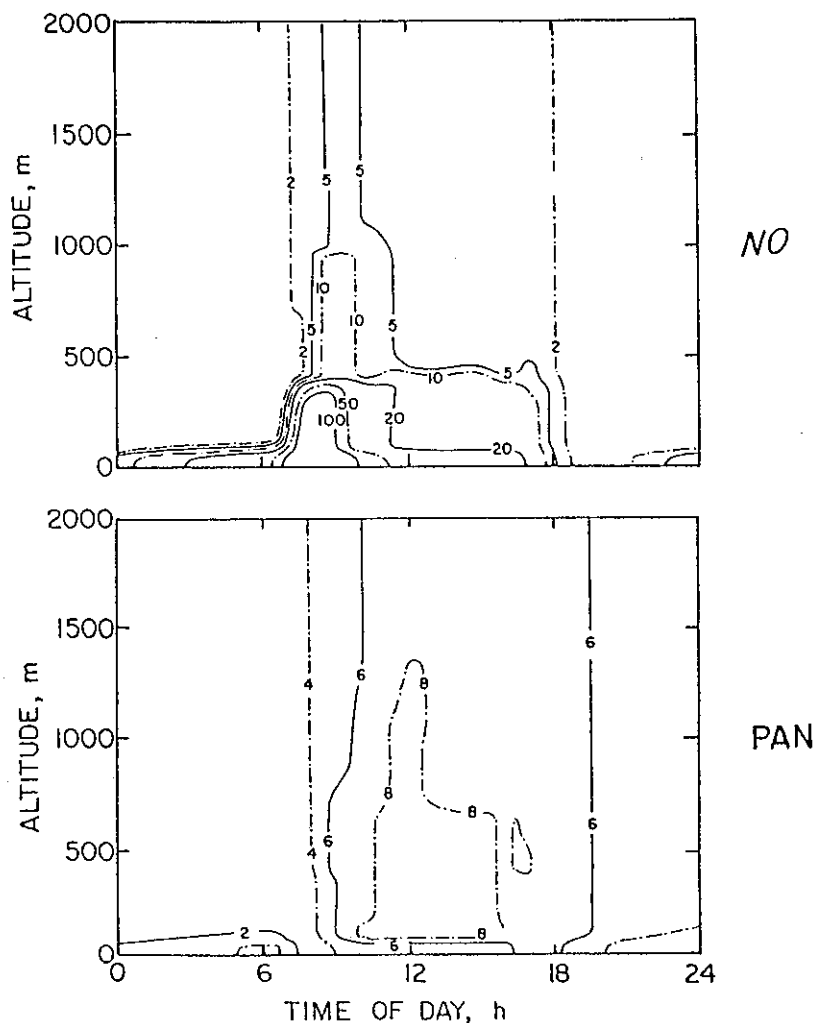
Fig. 8. Simulated concentrations of NO and PAN (ppt) in the PBL, as a function of altitude and time of day.

decomposition could make a significant contribution to the PBL NO$_x$ budget under meteorologically disturbed conditions when mass exchange between the PBL and the free troposphere is unusually rapid, and isoprene concentrations are depleted by dilution. Under the more typical conditions simulated here, however, decomposition of PAN does not have the potential to be an important source of NO$_x$ in the PBL.

Oxidation of NO$_x$ in the PBL takes place on a time scale of 1 day, and produces HNO$_3$ and organic nitrates which are subsequently removed by deposition (Table 8). The upward flux of NO$_x$ at 2000 m in the model is very small, indicating negligible export of biogenic NO$_x$ to the free troposphere. This inefficacy of NO$_x$ export from the PBL follows in part from the rapid oxidation of NO$_x$, and in part from the model assumption of 10 ppt NO$_x$ as an upper boundary condition at 2000 m (based on the NO measurements of A. L. Torres and K. R. Hooks, submitted manuscript, 1989). Model results thus imply that soil emissions make little contribution to the NO$_x$ budget above 2000 m. Possible sources of NO$_x$ above 2000 m include lightning [Crutzen et al., 1985] and thermal decomposition of PAN [Singh et al., this issue].

The concentrations of NO$_y$ measured at 39 m altitude during ABLE 2B averaged 450 ppt, with little diurnal variation [Bakwin et al., this issue (a)]. Only a small fraction of this NO$_y$ can be explained by the sum of the observed concentrations of NO, PAN, and HNO$_3$ [Bakwin et al., this issue (a); Singh et al., this issue;

[Talbot et al., this issue (a)]. Concentrations of NO$_2$, HNO$_2$, and biogenic organic nitrates predicted by the model from oxidation of biogenic NO are insufficient to account for the missing NO$_y$, particularly in the daytime (Table 9; Figure 9). We conclude that a large fraction of NO$_y$ over the forest must be contributed by compounds of non-biogenic origin, presumably organic nitrates transported from Manaus or from sources outside the Amazon Basin.

This hypothesis of a non-biogenic source for NO$_y$ was examined further by imposing a high concentration (1 ppb) of exogenous organic nitrates at the upper boundary of the model domain (2000 m). These organic nitrates were assumed to be chemically inert in the PBL, and to be removed by dry deposition to the forest. As shown in Figure 9, such an NO$_y$ source improves the simulation of the observed NO$_y$ concentrations. The exogenous organic nitrates in the model contribute 70% of the NO$_y$ observed at 39 m at noon, and 30% at midnight (Table 9). The lower fraction at night is due to NO$_x$ accumulation in the nighttime mixed layer, and depletion of organic nitrates by deposition to the canopy. The dry deposition of organic nitrates at night offsets the increasing levels of NO$_x$, thus explaining the lack of diurnal variation in NO$_y$ levels reported by Bakwin et al. [this issue (a)].

The NO$_y$ measurements of Bakwin et al. [this issue (a)] indicate higher NO$_y$ concentrations at 39 m than at 19 m, implying a net downward flux of NO$_y$ from the atmosphere to the canopy. This

TABLE 8. Budgets of Reactive Nitrogen Species in the PBL Air Column (30-2000 m)

Species	NO_x	PAN	RPAN	HNO_3	RNO_3^*	NO_y^*
Concentration, ppt	26	5.2	12	46	776	865
Sources and sinks, ppt d^{-1}						
Flux at canopy top (30 m)†	+33.4	-1.5	-1.5	-5.7	-106.1	-81.4
Wet deposition				-45.7		-45.7
Flux at 2000 m	-1.0	+3.6	-2.7	+35.8	+35.6	+71.3
PAN $\rightarrow NO_x$	+1.4	-1.4				
$NO_x \rightarrow$ RPAN	-6.0		+6.0			
$NO_x \rightarrow HNO_3$	-7.8			+7.8		
$NO_x \rightarrow RNO_3$	-16.2				+16.2	
Accumulation, ppt d^{-1}	+2.7	+0.7	+1.8	-7.8	-54.3	-55.8

Daily mean model values in the PBL air column (30-2000 m).
* Including exogenous organic nitrates (see text).
† Not including wet deposition.

TABLE 9. Simulated Concentrations of NO_y Species in Grid Cell 4 (30-40 m)

	Concentration, ppt	
	Noon	Midnight
NO	41	29
NO_2	66	291
PAN	5	2
RPAN	3	2
HNO_3	16	13
RNO_3^*	18	13
$RNO_3^†$	328	148
Total NO_y (model)‡	477	498
Total NO_y (observed)§	386±138	452±156

* Biogenic organic nitrates other than PAN or RPAN.
† Exogenous organic nitrates.
‡ Including exogenous organic nitrates.
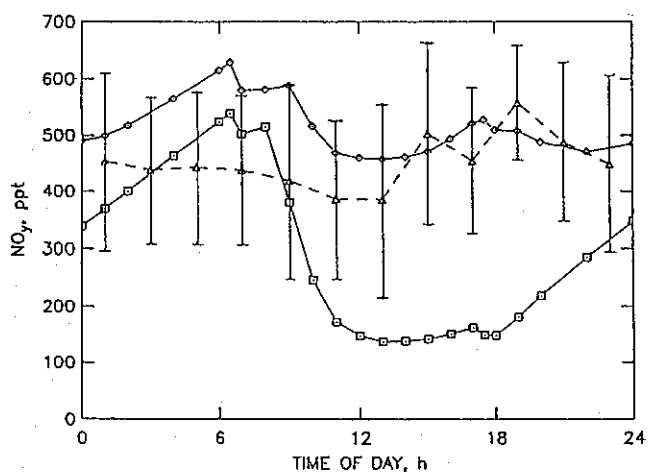§ At 39 m altitude [Bakwin et al., this issue (a)].

Fig. 9. Concentrations of NO_y just above the canopy, as a function of time of day. Model results for grid cell 4 (30-40 m) are shown as solid lines, for the simulation with and without exogenous organic nitrates (diamonds and squares, respectively). The observations of Bakwin et al. [this issue (a)] at 39 m are shown as the dashed line with error bars (mean ± standard deviation).

flux represents the sum of contributions from NO_y species removed by deposition (e.g., PAN, HNO_3, organic nitrates), partly balanced by soil emissions of NO. Bakwin et al. [this issue (a)] defined $NO_r = NO_y$-NO as the ensemble of NO_y species removed by deposition, and computed the dry deposition fluxes of NO_r on the basis of the observed NO_r gradients by assuming similarity with O_3 deposition. The ensemble of NO_r species defined in this manner includes NO_2, which in the model has a net flux upward at 40 m (Table 5), therefore, the assumption of similarity between NO_r and O_3 may not be fully warranted. The model simulation allows us to examine this question.

We compare in Figure 10 the NO_r fluxes computed by Bakwin et al. [this issue (a)] to the model values for the simulation with exogenous organic nitrates. Good agreement is found throughout the day, except that the high value computed by Bakwin et al. [this issue (a)] at 1300 LT is not reproduced by the model. Most of the NO_r flux in the model is contributed by the exogenous organic nitrates. The daily mean flux of NO_r in the model is -5.2×10^9 molecules $cm^{-2} s^{-1}$, compared to -6.5×10^9 molecules $cm^{-2} s^{-1}$ reported by Bakwin et al. [this issue (a)] (negative values indicate a downward flux). Correction for the NO_2 upward flux is small; the
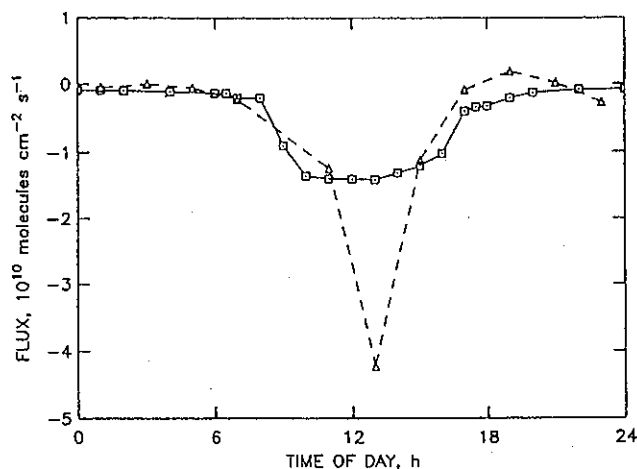

Fig. 10. Vertical flux of $NO_r = NO_y$-NO at 40 m, as a function of time of day. Model results (solid line) are compared to values computed from observed NO_r gradients [Bakwin et al., this issue (a)] (dashed line). Negative values indicate a downward flux.

daily mean flux of NO_r - NO_2 = NO_y - NO_x in the model is -5.8 x 10^9 molecules cm^{-2} s^{-1}, only 12% larger than the NO_r flux. The daily mean flux of NO_y in the model is -4.1 x 10^9 molecules cm^{-2} s^{-1}. These dry deposition fluxes can be compared to the mean NO_3^- wet deposition flux of 8.8 x 10^9 molecules cm^{-2} s^{-1} measured by *Andreae et al.* [this issue *(a)*] at the Embrapa sites during ABLE 2B. It appears that more NO_y is supplied to the forest by wet deposition than by dry deposition.

7. ODD HYDROGEN

Model concentrations of OH in the PBL are shown in Figure 11, and 24-hour average production and removal rates are listed in Table 10. Photolysis of O_3 accounts for 73% of the OH source, while reactions with isoprene and CO account for 58% of the sink. The OH concentration increases as the concentration of O_3 increases, and as the concentration of isoprene decreases; it is relatively insensitive to the concentration of NO_x as long as the latter is sufficiently low that photolysis of O_3 dominates over the reaction HO_2 + NO as a source of OH. Maximum OH concentrations of 2.4 x 10^6 molecules cm^{-3} are predicted at 1400 LT in the upper PBL, reflecting the relatively high levels of O_3 at that altitude and the low concentrations of isoprene. The OH concentrations near the canopy are much lower than aloft and show less diurnal variation, because the effect of increased O_3 photolysis at midday is offset by an increase in the isoprene concentration.
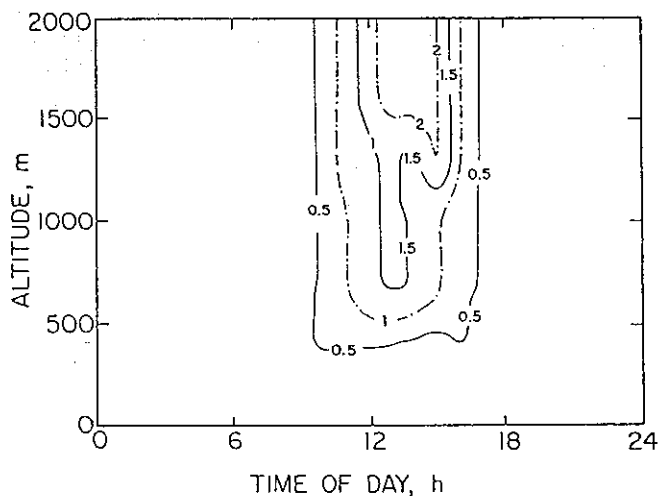

Fig. 11. Simulated concentrations of OH (10^6 molecules cm^{-3}) in the PBL, as a function of altitude and time of day.

It is convenient to group OH, HO_2, and RO_2 into one chemical family, odd hydrogen, and to refer to the ensemble of conversions between these species as the odd hydrogen cycle [*Logan et al.*, 1981]. The principal odd hydrogen source in the model is the photolysis of O_3, while the main sink is the formation of organic peroxides by peroxy-peroxy reactions (Table 11). Odd hydrogen cycling produces O_3 by the reactions

(R8) RO_2 + NO --> RO + NO_2

(R9) HO_2 + NO --> OH + NO_2

(R10) NO_2 + hv $\xrightarrow{O_2}$ NO + O_3
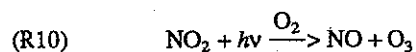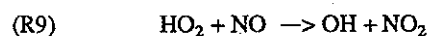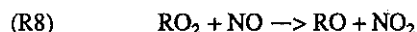
and consumes O_3 by the reaction

TABLE 10. Sources and Sinks of OH

	Values
Concentration, molecules cm^{-3}	3.5(5)
Sources, molecules $cm^{-3}s^{-1}$	
$O(^1D)$ + H_2O	6.7(5)
HO_2 + NO	1.0(5)
H_2O_2 + hv	5.8(4)
HO_2 + O_3	4.8(4)
ROOH + hv	4.1(4)
Total	9.2(5)
Sinks, molecules $cm^{-3}s^{-1}$	
Isoprene + OH	3.7(5)
CO + OH	1.6(5)
CH_4 + OH	9.3(4)
Methacrolein + OH	7.4(4)
Methylvinylketone + OH	4.7(4)
ROOH + OH	4.4(4)
CH_2O + OH	3.6(4)
H_2 + OH	2.4(4)
C_{3-5} aldehydes + OH	2.0(4)
Acetaldehyde + OH	1.3(4)
Miscellaneous*	3.9(4)
Total	9.2(5)

Daily mean model values in the PBL air column (30-2000 m). Read 3.5(5) as 3.5 x 10^5.

* Sum of minor sinks with individual rates < 1 x 10^4 molecules cm^{-3} s^{-1}.

(R11) HO_2 + O_3 --> OH + $2O_2$
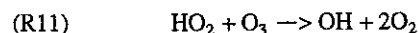
The RO radical produced in (R8) decomposes rapidly to yield HO_2 or a smaller $R'O_2$ molecule, conserving odd hydrogen. Under moderately polluted conditions (0.1-10 ppb NO_x) the rate of odd hydrogen cycling is much faster than the rate of odd hydrogen loss, and (R9) dominates over (R11), so that efficient photochemical production of O_3 takes place from a relatively small odd hydrogen source [cf. *Lin et al.*, 1988]. Over the Amazon forest, however, the concentration of NO_x is so low that odd hydrogen loss dominates over odd hydrogen cycling. Figure 12 illustrates the principal pathways of the odd hydrogen cycle in the simulation, for the lower PBL and for the upper PBL at noon. In both cases, odd hydrogen removal by formation of peroxides is faster than the conversion HO_2 --> OH that recycles odd hydrogen. As a result, photochemical production of O_3 is inefficient. Net photochemical loss of O_3 takes place in the upper PBL, as discussed further below.

8. OZONE

Model O_3 concentrations in the PBL range from 6 to 16 ppb, in harmony with the ABLE 2B aircraft observations (Figure 13). The simulated budget for O_3 in the PBL is regulated by downward transport from the free troposphere (supplying 1.2 ppb d^{-1} to the PBL) and losses from deposition to the canopy (-2.0 ppb d^{-1}) and photochemistry (-0.05 ppb d^{-1}). This budget implies a small net loss of O_3 in the PBL (-0.9 ppb d^{-1} on model day 3). A steady state concentration for O_3 would be approached after about 7 days,

but as we have previously pointed out (section 6) it is unlikely that the PBL could evolve such a long period without a major storm or intrusion of air from outside the Basin. We presume that these disturbances provide the missing source to close the O_3 budget in the PBL.

TABLE 11. Sources and Sinks of Odd Hydrogen

	Values
Concentration, molecules cm^{-3}	5.6(8)
Sources, molecules $cm^{-3}s^{-1}$	
$O(^1D) + H_2O$	6.7(5)
$CH_2O + hv$	1.3(5)
$ROOH + hv$	8.2(4)
Methylglyoxal + hv	6.5(4)
$H_2O_2 + hv$	5.8(4)
Total	1.0(6)
Sinks, molecules $cm^{-3}s^{-1}$	
RO_2+HO_2	7.7(5)
HO_2+HO_2	1.9(5)
$CH_3CO_3+CH_3O_2$	3.6(4)
$OH+HO_2$	1.5(4)
$CH_3O_2+CH_3O_2$	1.0(4)
Total	1.0(6)

Daily mean model values in the PBL air column (30-2000 m). The odd hydrogen family includes OH, HO_2, and all RO_2 species. Read 5.6(8) as 5.6 x 10^8.

Photochemical production and loss of O_3 in the PBL is strongly dependent on altitude, as shown in Figure 14. Photochemical loss of O_3 takes place above 500 m during the afternoon hours, while photochemical production takes place in the region immediately above the canopy where NO concentrations are relatively high. Comparison of Figures 8 and 14 indicates that the crossover NO concentration for O_3 production in the model is about 5 ppt. Photochemistry provides a net loss of O_3 for concentrations of NO below that level.

A simple analytical expression for the crossover NO concentration can be obtained by assuming that O_3 photolysis is the only odd hydrogen source, that RO_2 + NO is the only reaction producing O_3, and that formation of organic peroxides is the only odd hydrogen sink (see Figure 12). The O_3 yield Y per O_3 photolysis reaction (producing 2 odd hydrogen molecules) is then given by

$$Y = \frac{k_5[NO]}{k_6[HO_2]} \qquad (10)$$

where k_5 and k_6 are the rate constants for the reactions RO_2 + NO (R5) and RO_2 + HO_2 (R6), respectively. The crossover NO concentration for O_3 production is given by $Y = 1$, or

$$[NO] = \frac{k_6}{k_5}[HO_2] \qquad (11)$$

The concentration of HO_2 in the upper PBL at noon is 10 ppt, and the daytime average PBL concentration is 7 ppt, corresponding to NO crossover concentrations of 6 and 4 ppt, respectively. The factors regulating production and loss of O_3 over the Amazon forest
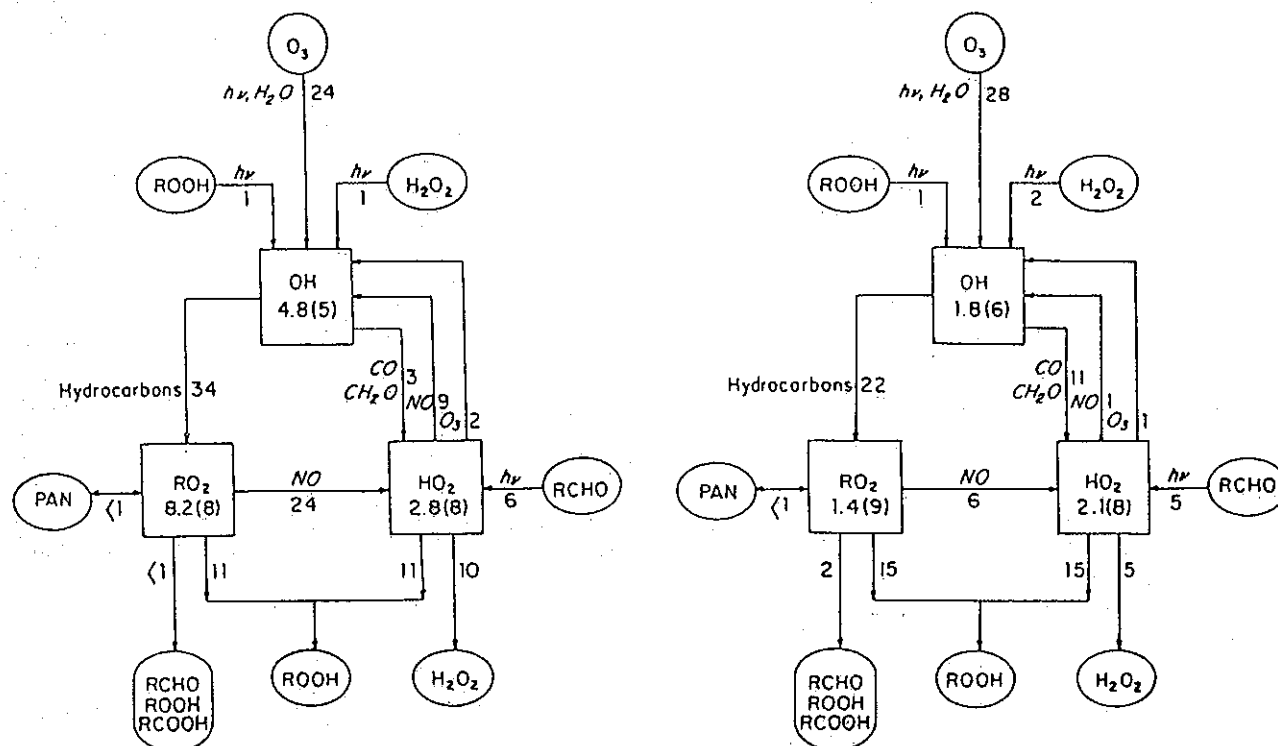

Fig. 12. Odd hydrogen cycle in the model at noon. The major reaction pathways are indicated. Concentrations are in units of molecules cm^{-3}, and transformation rates are in units of 10^5 molecules odd hydrogen cm^{-3} s^{-1}. Read 4.8(5) as 4.8x10^5 molecules cm^{-3}. Results for the lower PBL (40-500 m) are shown in the left panel. Results for the upper PBL (1500-2000 m) are shown in the right panel.
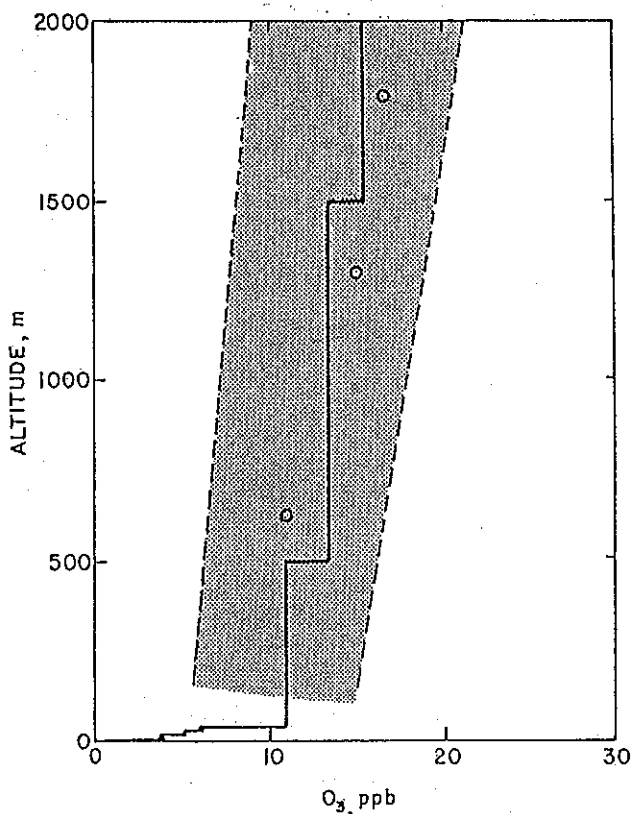
Fig. 13. Concentrations of O_3 in the PBL as a function of altitude. Model results at noon (solid line) are compared to the range of concentrations observed from aircraft during ABLE 2B (shaded area between dashed lines), and to the average of ozonesonde measurements (circles). Data from *Gregory et al.* [this issue] and *Browell et al.* [this issue].

are rather different than in the remote marine troposphere [*Fishman et al.*, 1979; *Logan et al.*, 1981; *Liu et al.*, 1983]. Production of RO_2 radicals plays a central role over the forest. Over the oceans, the key branch involves competition for HO_2 between O_3 and NO, and the NO crossover concentration for O_3 production is higher, about 10 ppt [*Fishman et al.*, 1979; *Chameides et al.*, 1987].

A major uncertainty in our analysis is the lack of kinetic data for reactions of RO_2 radicals. As shown in Table 12, C_5 hydroxy-RO_2 radicals produced from isoprene oxidation account for most of the RO_2 pool in the model. We investigated the sensitivity of O_3 production to the reactivities of RO_2 radicals by conducting a series of test simulations where the reaction rates of $>C_1$ RO_2 radicals with HO_2, NO, and NO_2 were taken to be (1) zero, (2) 10 times the value in the standard simulation. Results are summarized in Table 13. We find that photochemical loss of O_3 in the upper PBL at noon is remarkably insensitive to such variations in the kinetics of the RO_2 reactions. Ozone loss rates range from 91 ppt h^{-1} in the simulation with no $RCO_3 + NO_2$ reactions to 236 ppt h^{-1} in the simulation with no $RO_2 + HO_2$ reactions. This insensitivity is due in part to the inefficiency of odd hydrogen cycling at low NO_x concentrations (section 7), and in part to feedbacks between RO_2 and NO_x. For example, increasing the rate of the $RO_2 + HO_2$ reactions actually reduces photochemical loss because the depletion of RCO_3 radicals allows higher concentrations of NO_x to be sustained. Suppressing the $RO_2 + HO_2$ reactions depletes NO, raises the NO_2/NO ratio, and allows RCO_3 radicals to accumulate; the $NO_2/RPAN$ equilibrium is shifted towards RPAN, lowering levels of NO_x and enhancing photochemical loss.

Photochemistry in the lower PBL is somewhat more sensitive to the rates of RO_2 reactions, because NO_x levels are higher. For example, if rates for $RO_2 + HO_2$ are slow, then the atmosphere shifts from a regime of photochemical production of O_3 to photochemical loss (because of NO_x depletion). A similar shift occurs in the
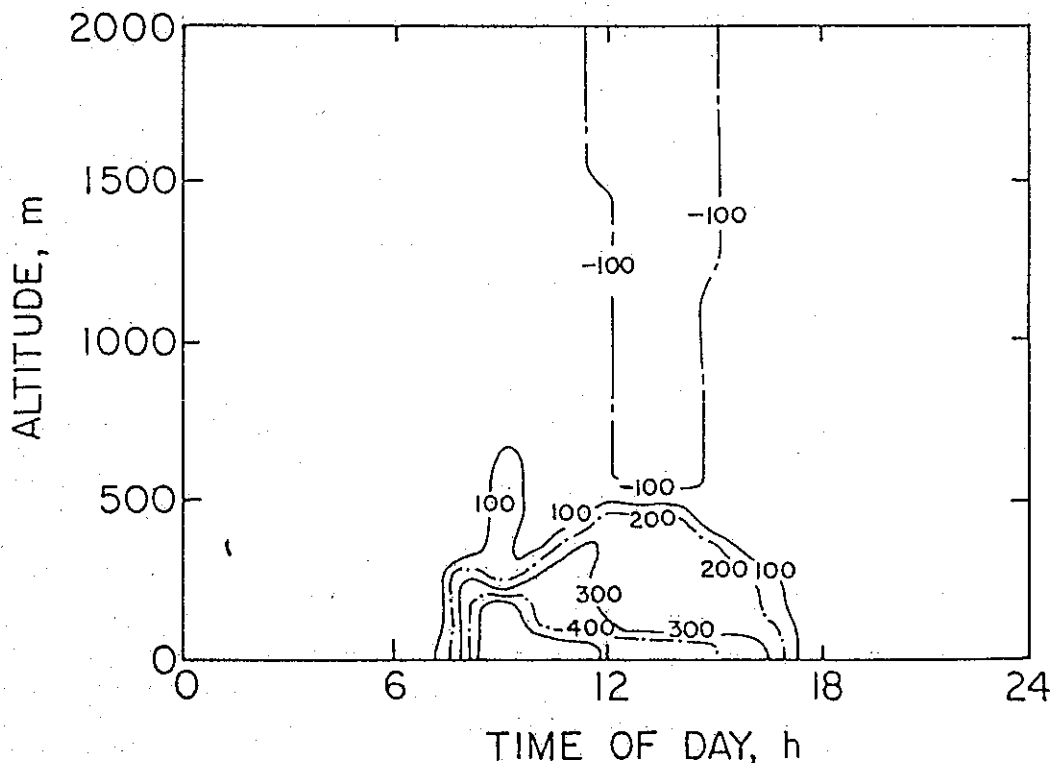

Fig. 14. Simulated photochemical production minus loss rates of O_3 (ppt h^{-1}), as a function of altitude and time of day.

TABLE 12. Major Contributors to the RO_2 Pool

Species	Total RO_2, %	Principal Source
$CH_2C(CH_3)CH(OO\bullet)CH_2OH$	26.4	Isoprene + OH
$CH_2CHC(CH_3)(OO\bullet)CH_2OH$	26.4	Isoprene + OH
$CH_2C(CH_3)CH(OH)CH_2OO\bullet$	11.3	Isoprene + OH
$CH_2CHC(CH_3)(OH)CH_2OO\bullet$	11.3	Isoprene + OH
$CH_3OO\bullet$	8.4	CH_4 + OH
$CH_3C(O)OO\bullet$	3.2	Methylglyoxal + hv
$CH_3C(O)CH(OO\bullet)CH_2OH$	2.0	Methylvinylketone + OH
$CH_3C(O)CH(OH)CH_2OO\bullet$	1.0	Methylvinylketone + OH
$CH_2CCH_3C(O)OO\bullet$	1.8	Methacrolein + OH
$CH_2(OH)CCH_3(OO\bullet)CHO$	1.8	Methacrolein + OH
$CH_2C(OO\bullet)C(OH)(CH_3)CHO$	1.8	Methacrolein + OH
$CH_2C(CH_3)OO\bullet$	1.3	Methacrolein + OH
$CH_3CH_2OO\bullet$	1.1	RCO_3 + NO
Miscellaneous	2.2	
Total	100.0	

Model results for grid cell 5 (40-500 m) at noon.

TABLE 13. Sensitivity of Model Results to the Rates of RO_2 Reaction

	[NO], ppt	[NO_x], ppt	[O_3], ppb	[RO_2]	[HO_2]	[OH]	$(P-L)O_3$ ppt h^{-1}
Grid cell 5 (40-500 m)							
Standard	16.4	54.6	11.3	8.2(8)	2.8(8)	4.8(5)	+272
$k(RO_2 + HO_2)=0$	0.2	10.1	10.0	2.4(10)	3.2(8)	3.2(5)	-61
$k(RO_2 + HO_2)\times10$	28.5	71.4	10.7	3.2(8)	1.1(8)	4.3(5)	+133
$k(RO_2 + NO)=0$	36.1	63.0	9.5	1.2(10)	1.0(7)	3.0(5)	-151
$k(RO_2 + NO)\times10$	10.9	54.6	12.2	2.9(8)	4.3(8)	5.2(5)	+424
$k(RCO_3 + NO_2)=0$	16.8	58.8	11.3	8.1(8)	2.8(8)	5.0(5)	+287
$k(RCO_3 + NO_2)\times10$	12.6	42.0	10.4	8.9(8)	2.5(8)	4.1(5)	+182
Grid cell 7 (1500-2000 m)							
Standard	3.1	11.2	15.5	1.4(9)	2.1(8)	1.8(6)	-138
$k(RO_2 + HO_2)=0$	0.05	1.7	14.4	2.8(10)	2.9(8)	1.7(6)	-236
$k(RO_2 + HO_2)\times10$	7.3	19.4	15.1	4.8(8)	1.4(8)	1.9(6)	-126
$k(RO_2 + NO)=0$	4.5	10.2	14.1	6.7(9)	5.0(7)	1.7(6)	-186
$k(RO_2 + NO)\times10$	1.0	10.2	16.0	9.2(8)	2.9(8)	1.8(6)	-105
$k(RCO_3 + NO_2)=0$	4.7	17.0	15.6	1.2(9)	2.4(8)	1.9(6)	-91
$k(RCO_3 + NO_2)\times10$	0.3	1.6	14.5	2.9(9)	9.8(7)	1.6(6)	-224

Results at noon. In the sensitivity simulations the reaction rates for >C_1 RO_2 radicals are modified to be either zero or 10 times the value in the standard simulation. $(P-L)O_3$ is the net photochemical production rate of O_3. Read 8.2(8) as 8.2×10^8.

absence of RO_2 + NO reactions (because HO_2 is then depleted by RO_2 + HO_2 reactions). In the simulation with no RO_2 + HO_2 reactions the noontime NO concentration in the lower PBL is 0.2 ppt, whereas the concentrations observed at that altitude by A. L. Torres and K. R. Hooks (submitted manuscript, 1989) were of order 10 ppt. The observation of detectable NO in the lower PBL thus provides indirect evidence for the occurrence of RO_2 + HO_2 reactions, or at least for a RO_2 sink other than reactions with NO and NO_2.

Other possible sinks for >C_1 RO_2 radicals, which are not considered in the model, include the reactions with O_3 and with other RO_2 radicals. *Atkinson and Lloyd* [1984] have argued that the RO_2 + O_3 reactions should be negligibly slow. The RO_2 + RO_2 reactions could however be important; this importance is suggested by model results for CH_3CO_3, which indicate that the reactions of CH_3CO_3 with itself and with CH_3O_2 amount together to a sink for CH_3CO_3 comparable to reaction with HO_2. We did not attempt to consider the sensitivity of model results to the RO_2 + RO_2 reactions because of the large uncertainty regarding the reaction products. Obviously, our model study points to the need for further laboratory work on these reactions.

9. SENSITIVITY OF MODEL RESULTS TO HYDROCARBON LEVELS

Zimmerman et al. [1988] found that several primary NMHCs other than isoprene were present at significant concentrations over the Amazon forest during the dry season. Most of these NMHCs appeared to originate from biomass burning, hence the concentrations in the wet season would probably be much lower. We conducted a sensitivity model simulation assuming NMHC concentrations fixed at the mean values reported by *Zimmerman et al.* [1988] for unpolluted conditions. These concentrations were 0.37 ppb propane, 0.17 ppb butane, 0.32 ppb pentane, 0.10 ppb higher alkanes, 1.0 ppb ethylene, 0.31 ppb propene, 0.09 ppb benzene, 0.74 ppb toluene, and 0.09 ppb xylene.

Results from the simulation with added NMHCs are compared to the standard simulation in Table 14. Differences are in general small. The addition of NMHCs decreases the concentrations of

OH and HO_2, and increases the concentration of RO_2 radicals, as would be expected. The concentration of NO_x decreases by 12%, partly because of the increase in RCO_3 concentrations which facilitates the formation of RPAN compounds, and partly because of nighttime reactions of NO_3 with cresols and phenols. The decrease in NO_x levels leads to enhanced photochemical loss of O_3 in the simulation with added NMHCs, -0.3 ppb d^{-1} as compared to -0.05 ppb d^{-1} in the standard simulation. Photochemical consumption remains nevertheless a small sink for O_3 in the PBL compared to deposition.

Computed rates for photochemical production of CO are remarkably unsensitive to NMHC levels. This result follows largely from the low concentrations of NO, which prevent odd hydrogen cycling. The rate of hydrocarbon oxidation is limited by the supply of OH, which is in turn regulated by O_3 photolysis (Figure 12). The production of CO over the Amazon forest appears therefore to be dependent not on the supply of NMHCs but rather on rates for O_3 photolysis, levels of H_2O, and CO yields from NMHC oxidation. As pointed out in section 6, the CO yields are expected to be low because water-soluble hydrocarbon intermediates are removed by wet deposition.

10. CONCLUSIONS

The atmospheric composition observed over the Amazon forest during the wet season reflects influences from deposition to the forest canopy, biogenic sources of NO and hydrocarbons, exchange with the free troposphere, and influx from polluted regions. We analyzed the contributions from these various influences to the budgets of chemically reactive species, using a photochemical model for the PBL (0-2000 m) with detailed simulation of deposition processes in the canopy. Results indicate that only 19% of NO_x emitted by soil is exported to the PBL on a 24-hour average basis; the balance is removed by deposition of NO_2 to vegetation. The small fraction of NO_x soil emissions exported from the canopy is nevertheless sufficient to account for the NO

TABLE 14. Sensitivity of Model Results to Hydrocarbon Levels

	Standard Simulation	Simulation With Added NMHCs
$Molecules\ cm^{-3}$		
OH	3.5 (5)	2.2 (5)
HO_2	8.2 (7)	7.9 (7)
CH_3CO_3	1.5 (7)	1.6 (7)
RO_2	4.7 (8)	6.5 (8)
Parts per Trillion		
NO	3.4	2.8
NO_x	26	23
PAN	5.2	4.3
RPAN	12	14
Parts per Billion		
CO	90.5	91.2

Daily mean concentrations in the PBL air column (30-2000 m). Read 3.5(5) as 3.5×10^5.

levels observed in the PBL, implying that soil emissions regulate the levels of NO_x in the lower atmosphere. Decomposition of PAN transported from the free troposphere provides only a small source of NO_x to the PBL, as compared to soil emission, because mass exchange between the PBL and the free troposphere is relatively slow. Soil emissions of NO can account for only a small fraction of total reactive nitrogen (NO_y) observed over the forest, and we speculate that organic nitrates transported from sources outside the Amazon Basin make a large contribution to the NO_y budget. Ventilation of biogenic NO_x from the PBL to higher altitudes is negligible, indicating that NO_x above 2000 m must be supplied by a different source, e.g., decomposition of PAN as suggested by *Singh et al.* [this issue].

Photochemical activity in the atmosphere over the Amazon forest is limited by the low concentrations of NO_x. Oxidation of isoprene is slow and yields principally organic peroxides that are removed by wet and dry deposition. The observed enhancements of CO in the PBL cannot be attributed to oxidation of isoprene or other hydrocarbons and probably result from direct emission of CO by the forest ecosystem.

Concentrations of O_3 in the PBL reflect largely a balance between supply from the free troposphere and removal by deposition to vegetation. Ozone is photochemically produced just above the canopy, and photochemically consumed in the upper PBL; overall, the net effect of photochemistry on O_3 levels in the PBL is small. This result contrasts with dry season conditions, when NO concentrations are sufficiently high to provide a vigorous photochemical source of O_3 in the PBL.

REFERENCES

Andreae, M.O., et al., Biomass-burning emissions and associated haze layers over Amazonia, *J. Geophys. Res.*, *93* 1509-1527, 1988.

Andreae, M.O., R.W. Talbot, H. Berresheim, and K.M. Beecher, Precipitation chemistry in central Amazonia, *J. Geophys. Res.*, this issue *(a)*.

Andreae, M.O., H. Berresheim, H. Bingemer, D.J. Jacob, and R.W. Talbot, The atmospheric sulfur cycle over the Amazon Basin, 2, Wet season, *J. Geophys. Res.*, this issue *(b)*.

Atkinson, R., and A.L. Lloyd, Evaluation of kinetic and mechanistic data for modeling of photochemical smog, *J. Phys. Chem. Ref. Data*, *13*, 315-444, 1984.

Bakwin, P.S., S.C. Wofsy, and S.-M. Fan, Measurements of reactive nitrogen oxides (NO_y) within and above a tropical forest canopy in the wet season, *J. Geophys. Res.*, this issue *(a)*.

Bakwin, P.S., S.C. Wofsy, S.-M. Fan, M. Keller, S. Trumbore, and J. M. da Costa, Emission of nitric oxide (NO) from tropical forest soils and exchange of NO between the forest canopy and atmospheric boundary layers, *J. Geophys. Res.*, this issue *(b)*.

Browell, E. V., G. L. Gregory, R. C. Harriss, and V. W. J. H. Kirchhoff, Ozone and aerosol distributions over the Amazon Basin during the wet season, *J. Geophys. Res.*, this issue.

Browell, E.V., G.L. Gregory, R.C. Harriss, and V.W.J.H. Kirchhoff, Tropospheric ozone and aerosol distributions across the Amazon Basin, *J. Geophys. Res.*, *93*, 1431-1451, 1988.

Chameides, W.L., D.D. Davis, M.O. Rodgers, J. Bradshaw, S. Sandholm, G. Sachse, G. Hill, G. Gregory, and R. Rasmussen, Net ozone photochemical production over the eastern and central North Pacific as inferred from GTE/CITE 1 observations during dall 1983, *J. Geophys. Res.*, *92*, 2131-2152, 1987.

Chatfield, R.B., and A.C. Delany, Convection links biomass burning to increased tropical ozone: However, models will typically overpredict O_3, *J. Geophys. Res.*, in press, 1990.

Crutzen, P.J., The role of NO and NO_2 in the chemistry of the troposphere and stratosphere, *Annu. Rev. Earth Planet. Sci.*, *7*, 443-472, 1979.

Crutzen, P.J., A.C. Delany, J. Greenberg, P. Haagenson, L. Heidt, R. Lueb, W. Pollock, W. Seiler, A. Wartburg, and P. Zimmerman, Tropospheric chemical composition measurements in Brazil during the dry season, *J. Atmos. Chem.*, *2*, 233-256, 1985.

Dalluge, R., R.A. Rasmussen, and M.A.K. Khalil, Isoprene fluxes from ABLE, *Eos Trans. AGU*, *68*, 1220, 1987.

Fan, S.-M., S.C. Wofsy, P.S. Bakwin, and D.J. Jacob, Atmosphere-biosphere exchange of CO_2 and O_3 in the central Amazon forest, *J. Geophys. Res.*, this issue.

Fishman, J., S. Solomon, and P.J. Crutzen, Observational and theoretical evidence in support of a significant in-situ photochemical source of tropospheric ozone, *Tellus*, *31*, 432-446, 1979.

Fitzjarrald, D.R., and K.E. Moore, Mechanisms of nocturnal exchange between the rain forest and the atmosphere, *J. Geophys. Res.*, this issue.

Fitzjarrald, D.R., B.L. Stormwind, G. Fisch, and O.M.R. Cabral, Turbulent transport observed just above the Amazon forest, *J. Geophys. Res.*, *93* 1551-1563, 1988.

Fitzjarrald, D.R., K.E. Moore, O.M.R. Cabral, J. Scolar, A.O. Manzi, and L.D. de Abreu Sa, Daytime turbulent exchange between the Amazon forest and the atmosphere, *J. Geophys. Res.*, this issue.

Gregory, G.L., E.V. Browell, and L.S. Warren, Boundary layer ozone: an airborne survey across the Amazon Basin, *J. Geophys. Res.*, *93*, 1452-1468, 1988.

Gregory, G.L., E. Browell, L.S. Warren, and C.H. Hudgins, Amazon Basin ozone and aerosol: wet season observations, *J. Geophys. Res.*, this issue.

Harriss, R.C., et al., The Amazon Boundary Layer Experiment (ABLE 2B): Wet season 1987, *J. Geophys. Res.*, this issue *(a)*.

Harriss, R.C., G.W. Sachse, G.F. Hill, G.L. Gregory, and J. Fishman, Carbon monoxide over the Amazon Basin during the 1987 wet season, submitted to *J. Geophys. Res.*, this issue *(b)*.

Jacob, D.J., and S.C. Wofsy, Photochemistry of biogenic emissions over the Amazon forest, *J. Geophys. Res.*, *93*, 1477-1486, 1988.

Jacob, D.J., and P.S. Bakwin, Cycling of NO_x in tropical forest canopies and its implications for the global source of biogenic NO_x to the atmosphere, in *Microbial Production and Consumption of Greenhouse Gases*, edited by W.B. Whitman, American Society of Microbiology, Washington, D.C., in press, 1990.

Jones, H.G., *Plants and Microclimate*, Cambridge University Press,, New York, 1983.

Kasting, J.F., and H.B. Singh, Nonmethane hydrocarbons in the troposphere: impact on the odd hydrogen and odd nitrogen chemistry, *J. Geophys. Res., 91*, 13,239-13,256, 1986.

Keller, M., D.J. Jacob, S.C. Wofsy, and R.C. Harriss, Effects of tropical deforestation on global and regional atmospheric chemistry, *Clim. Change*, in press, 1990.

Kirchhoff, V.W.J.H., and E.V. Marinho, Surface carbon monoxide measurements in Amazonia, *J. Geophys. Res.*, this issue.

Kirchhoff, V.W.J.H., A.W. Setzer, and M.C. Pereira, Biomass burning in Amazonia: Seasonal effects on atmospheric O$_3$ and CO, *Geophys. Res. Lett., 16*, 469-472, 1989.

Kirchhoff, V.W.J.H., I.M.O. da Silva, and E.V. Browell, Ozone measurements in Amazonia: Dry season vs. wet season, *J. Geophys. Res.*, this issue.

Kousky, V.E., and M.T. Kagano, A climatological study of the tropospheric circulation over the Amazon region, *Acta Amazonica, 11*, 743-758, 1981.

Lamb, B., A. Guenther, D. Gay, and H. Westberg, A national inventory of biogenic hydrocarbon emissions, *Atmos. Environ., 21*, 1695-1705, 1987.

Lin, X., M. Trainer, and S.C. Liu, On the nonlinearity of tropospheric ozone production, *J. Geophys. Res., 93*, 15,879-15,888, 1988.

Liu, S.C., M. McFarland, D. Kley, O. Zafiriou, and B. Huebert, Tropospheric NO$_x$ and O$_3$ budgets in the equatorial Pacific, *J. Geophys. Res., 88*, 1360-1368, 1983.

Lloyd, A.C., R. Atkinson, F.W. Lurmann, and B. Nitta, Modeling potential ozone impacts from natural hydrocarbons, I, Development and testing of a chemical mechanism for the NO$_x$-air photooxidations of isoprene and α-pinene under ambient conditions, *Atmos. Environ., 17*, 1931-1950, 1983.

Logan, J.A., M.J. Prather, S.C. Wofsy, and M.B. McElroy, Tropospheric chemistry: a global perspective, *J. Geophys. Res., 86*, 7210-7254, 1981.

Lowe, D.C., and U. Schmidt, Formaldehyde measurements in the nonurban atmosphere, *J. Geophys. Res., 88*, 10,844-10,858, 1983.

Lurmann, F.W., A.C. Lloyd, and R. Atkinson, A chemical mechanism for use in long-range transport/acid deposition computer modeling, *J. Geophys. Res., 91*, 10,905-10,936, 1986.

Menzel, W.P., T. J. Schmit, and D. P. Wylie, Cloud characteristics over central Amazonia during GTE/ABLE 2B derived from multispectral visible and infrared spin scan radiometer atmospheric sound observations, *J. Geophys. Res.*, this issue.

Meyers, T.P., and D.D. Baldocchi, A comparison of models for deriving dry deposition fluxes of O$_3$ and SO$_2$ to a forest canopy, *Tellus, 40B*, 270-284, 1988.

Moortgaat, G.K., B. Veyret, and R. Lesclaux, Absorption spectrum and kinetics of reactions of the acetylperoxy radical, *J. Phys. Chem., 93*, 2362-2368, 1989a.

Moortgaat, G.K., B. Veyret, and R. Lesclaux, Kinetics of the reaction of HO$_2$ with CH$_3$C(O)O$_2$ in the temperature range 253-368K, *Chem. Phys. Lett., 160*, 443-447, 1989b.

Neitzert, V., and W. Seiler, Measurement of formaldehyde in clean air, *Geophys. Res. Lett., 8*, 79-82, 1981.

Parsons, T.R., M. Takahashi, and B. Hargrave, *Biological Oceanographic Processes*, 2nd ed., pp. 73-74, Pergamon Press, New York, 1977.

Rasmussen, R.A., and M.A.K. Khalil, Isoprene over the Amazon Basin, *J. Geophys. Res., 93*, 1417-1421, 1988.

Richtmeyer, R.D., *Difference Methods for Initial Value Problems*, p. 101, Wiley-Interscience, New York, 1957.

Roberts, J., O.M.R. Cabral, and L.F. De Aguiar, Stomatal and boundary layer conductances measured in an Amazonian Terra Firme rain forest, *J. Appl. Ecol., 27*, 336-353, 1990.

Scala, J.R., et al., Cloud draft structure and trace gas transport, *J. Geophys. Res.*, this issue.

Seiler, W., The influence of the biosphere on the atmospheric CO and H$_2$ cycles, in *Environmental Biogeochemistry and Geomicrobiology*, vol. 3, edited by W.E. Krumbein, pp. 773-810, Ann Arbor Science Publishers, Ann Arbor, Michigan, 1978.

Shreffler, J.H., Factors affecting dry deposition of SO$_2$ on forests and grasslands, *Atmos. Environ., 12*, 1497-1503, 1978.

Shuttleworth, W.J., et al., Observations of radiation exchange above and below Amazonian forest, *Q. J. R. Meteorol. Soc., 110*, 1163-1169, 1984.

Singh, H.B., Reactive nitrogen in the troposphere, *Environ. Sci. Technol. 21*, 320-327, 1987.

Singh, H.B., D. Herlth, D. O'Hara, L. Salas, A. L. Torres, G. L. Gregory, G. W. Sachse, and J. F. Kasting, Atmospheric peroxyacetyl nitrate measurements over the Brazilian Amazon Basin during the wet season: Relationship with nitrogen oxides and ozone, *J. Geophys. Res.*, this issue.

Snider, J.R., and G.A. Dawson, Tropospheric light alcohols, carbonyls, and acetonitrile: Concentrations in the southwestern United States and Henry's law data, *J. Geophys. Res., 90*, 3797-3805, 1985.

Talbot, R.W., M.O. Andreae, H. Berresheim, P. Antaxo, M. Garstang, R.C. Harriss, K.M. Beecher, and S.M. Li, Aerosol chemistry during the wet season in central Amazonia: The influence of long-range transport, *J. Geophys. Res.*, this issue *(a)*.

Talbot, R.W., M.O. Andreae, H. Berresheim, D.J. Jacob, and K.M. Beecher, Sources and sinks of formic, acetic, and pyruvic acids over central Amazonia 2, Wet season, *J. Geophys. Res.*, this issue *(b)*.

Tingey, D.T., M. Manning, L.C. Grothaus, and W.F. Burns, The influence of light and temperature on isoprene emission rates from live oak, *Physiol. Plant., 47*, 112-118, 1979.

Torres, A.L., and H. Buchan, Tropospheric nitric oxide measurements over the Amazon Basin, *J. Geophys. Res., 93*, 1396-1406, 1988.

Trumbore, S.E., M. Keller, S.C. Wofsy, and J.M. da Costa, Measurements of soil and canopy exchange rates in the Amazon rain forest using ^{222}Rn, *J. Geophys. Res.*, this issue.

Verstraete, M.M., Radiation transfer in plant canopies: transmission of direct solar radiation and the role of leaf orientation, *J. Geophys. Res., 92*, 10,985-10,995, 1987.

Wesely, M.L., Improved parameterizations for surface resistance to gaseous dry deposition in regional-scale, numerical models, *Atmos. Environ., 23*, 1293-1304, 1989.

Zimmerman, P.R., R.B. Chatfield, J. Fishman, P.J. Crutzen, and P.L. Hanst, Estimates on the production of CO and H$_2$ from the oxidation of hydrocarbon emissions from vegetation, *Geophys. Res. Lett., 5*, 679-682, 1978.

Zimmerman, P.R., J.P Greenberg, and C.E. Westberg, Measurements of atmospheric hydrocarbons and biogenic emission fluxes in the Amazon boundary layer, *J. Geophys. Res., 93*, 1407-1416, 1988.

D. J. Jacob and S. C. Wofsy, Department of Earth and Planetary Sciences and Division of Applied Sciences, Harvard University, Cambridge, MA 02138.